

A Novel Approach for the Development of Selective Cdk4 Inhibitors: Library Design Based on Locations of Cdk4 Specific Amino Acid Residues

Teruki Honma,* Takashi Yoshizumi, Noriaki Hashimoto, Kyoko Hayashi, Nobuhiko Kawanishi, Kazuhiro Fukasawa, Tohru Takaki, Chinatsu Ikeura, Mari Ikuta, Ikuko Suzuki-Takahashi, Takashi Hayama, Susumu Nishimura, and Hajime Morishima

Banyu Tsukuba Research Institute in collaboration with Merck Research Laboratories, Okubo-3, Tsukuba 300-2611, Ibaraki, Japan

Received July 17, 2001

Identification of a selective inhibitor for a particular protein kinase without inhibition of other kinases is critical for use as a biological tool or drug. However, this is very difficult because there are hundreds of homologous kinases and their kinase domains including the ATP binding pocket have a common folding pattern. To address this issue, we applied the following structure-based approach for designing selective Cdk4 inhibitors: (1) identification of specifically altered amino acid residues around the ATP binding pocket in Cdk4 by comparison of 390 representative kinases, (2) prediction of appropriate positions to introduce substituents in lead compounds based on the locations of the altered amino acid residues and the binding modes of lead compounds, and (3) library design to interact with the altered amino acid residues supported by *de novo* design programs. Accordingly, Asp99, Thr102, and Gln98 of Cdk4, which are located in the p16 binding region, were selected as first target residues for specific interactions with Cdk4. Subsequently, the 5-position of the pyrazole ring in the pyrazol-3-ylurea class of lead compound (**2a**) was predicted to be a suitable position to introduce substituents. We then designed a chemical library of pyrazol-3-ylurea substituted with alkylaminomethyl groups based on the output structures of *de novo* design programs. Thus we identified a highly selective and potent Cdk4 inhibitor, **15b**, substituted with a 5-chloroindan-2-ylaminomethyl group. Compound **15b** showed higher selectivity on Cdk4 over those on not only Cdk1/2 (780-fold/190-fold) but also many other kinases (>430-fold) that have been tested thus far. The structural basis for Cdk4 selective inhibition by **15b** was analyzed by combining molecular modeling and the X-ray analysis of the Cdk4 mimic Cdk2–inhibitor complex. The results suggest that the hydrogen bond with the carboxyl group of Asp99 and hydrophobic van der Waals contact with the side chains of Thr102 and Gln98 are important. Compound **15b** was found to cause cell cycle arrest of the Rb(+) cancer cell line in the G₁ phase, indicating that it is a good biological tool.

Introduction

Cyclins and cyclin-dependent kinases (Cdks) play important roles in regulation of the cell cycle.¹ In particular, D-type cyclins, which have been shown to be amplified or overexpressed in several tumor cells,² associate with Cdk4/6 to activate their phosphorylation activity. Cyclin D–Cdk4/6 complexes phosphorylate the retinoblastoma protein (pRB) and regulate the cell cycle during G₁/S transition.³ Loss of function or deletion of p16^{ink4a} (endogenous Cdk4/6 specific inhibitor protein) frequently occurs in clinical cancer cells.⁴ Thus, selective Cdk4/6 inhibitors should be useful as a new class of cytostatic antitumor agents.⁵

In the previous paper, we reported the structure-based lead generation of a novel diarylurea class of potent Cdk4 inhibitors.⁶ The Cdk4 homology model was constructed according to X-ray analysis of the activated form of Cdk2.⁷ Using this model, we applied a new *de novo* design strategy⁸ to generate new scaffold candidates. As a result, a diarylurea class of scaffold was identified, and a potent compound **1** (IC₅₀ = 0.042 μM) was obtained through modifications based on the pre-

dicted binding mode. The predicted binding mode was validated by the X-ray analysis of the Cdk2–**1** complex (PDB ID: 1GIH)⁹ and the structure–activity relationship (SAR) (Figure 1).

Compound **1** showed good Cdk4 inhibitory activity and moderate selectivity (>50-fold) over other kinases except the Cdk family (Table 1). However, **1** also inhibited Cdk family kinases in addition to Cdk4/6, namely Cdk1 and Cdk2, with comparable IC₅₀ values. In the predicted binding mode, compound **1** appeared to form hydrogen bonds with the main chain of Val96 and the side chain amino group of Lys35. Although Val96 in Cdk4 is replaced by Leu in Cdk1/2, the main chain atoms are located in the same position. Lys35 is conserved in Cdk4 and Cdk1/2. Additionally, since the sequence identities between Cdk4 and Cdk1/2 are high (43%/45%), the shapes of their ATP binding pockets were predicted to be very similar. Therefore, it was assumed that compound **1** does not achieve any specific interactions with Cdk4 against Cdk1/2. The selectivity of Cdk4(6) over Cdk1/2 is thought to be critical for the arrest of the cell cycle in the G₁ phase because Cdk1 and Cdk2 regulate the transition to other phases of the cell cycle.¹⁰ To suppress tumor growth, G₁ arrest is expected to reduce the stress of normal cells other than

* To whom correspondence should be addressed. Tel: 81-298-77-2000. Fax: 81-298-77-2029. E-mail: honmatr@banyu.co.jp.

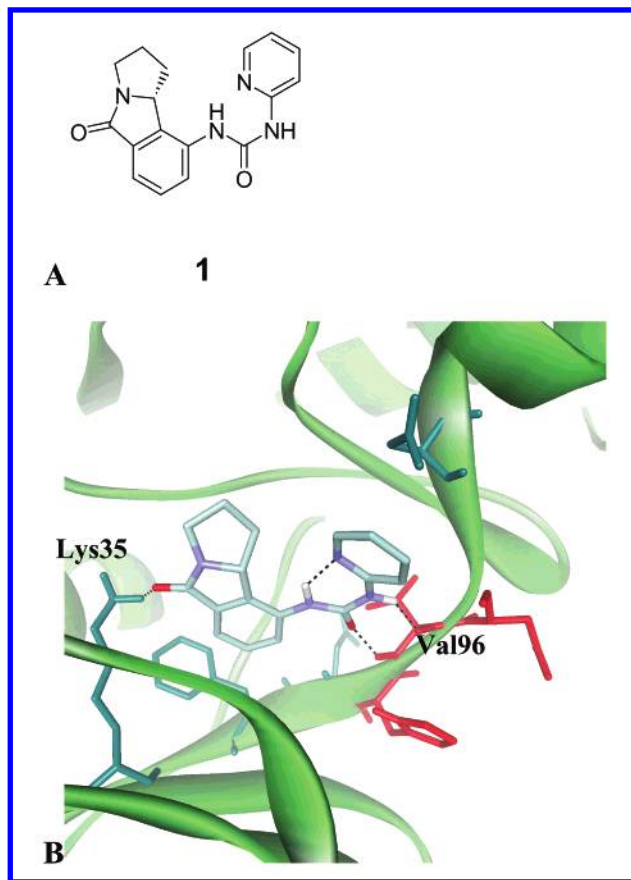


Figure 1. Structure and binding mode of compound **1**. A: structure of compound **1**. B: the binding mode of **1** in the Cdk4 homology model based on X-ray analysis of the Cdk2–1 complex (PDB ID: 1GIH).⁹ Green residues: residues conserved in Cdk4 and Cdk1/2. Red residues: residues altered in Cdk1/2. Broken lines: predicted hydrogen bonds.

arrest in other phases because normal cells are usually resting in the G_0 - G_1 phase.¹¹ In this report, we tried to design Cdk4 selective inhibitors with effects over both Cdk1/2 and other kinases.

Enhancement of selectivity for the target protein over its highly homologous counterparts is not feasible because there are few differences in the protein surface of the ligand binding sites. Recently, successful examples of the development of such selective compounds have been reported; these processes used structural information about critical differences in amino acid residues and/or conformations between the target proteins (MMP-13, PTP1B, and COX-2) and their counterparts.¹² However, in the case of protein kinases, it is more difficult to improve selectivity for a target protein because there are hundreds of homologous kinases in the superfamily.¹³ To overcome this problem, we initially identified specific amino acid residues around the ATP binding pocket of Cdk4 by comparing the amino acid sequences of 390 representative kinases. Subsequently, a chemical library was designed using this information about the locations of these amino acid residues and the binding mode of compound **1** to achieve specific interactions with Cdk4, discriminating against interactions with other kinases.

Results and Discussion

Identification of Specifically Altered Amino Acid Residues around the ATP Binding Pocket of Cdk4. First, we performed a 3D superposition of the structural model of Cdk4 bound with compound **1** and the X-ray structure of Thr160 phosphorylated Cdk2–cyclin A–ATP γ S reported by A. A. Russo et al.⁷ We then chose 39 amino acid residues in the Cdk4 model which are located within 7 Å of the ATP γ S molecule in the Cdk2 (these residues are shown in Figure 2).

Table 1. Potency and Cdk4 Selectivity of Compound **1** for Representative Kinases

	Hanks' classification	Kinase	IC ₅₀ (μM)	Cdk4 selectivity (-fold)	
Ser/Thr kinase	CMGC	cyclin D-Cdk4	0.042	1.0	
		cyclin D-Cdk6	0.071 ^a	1.7 ^a	
		cyclin B-Cdk1	0.120	2.9	
		cyclin A-Cdk2	0.078	1.9	
	AGC	PKA	>20	>480	
		PKC	>20	>480	
		PKBα (Akt1)	>10	>240	
		CaMK	CaMK II	>10	>240
		CMGC	p38α	>10	>240
			ERK1	>10	>240
OPK	MEK1	>10	>240		
Tyrosine kinase	PTK	Src	>5.0 ^a	>120 ^a	
		Lck	2.3 ^a	55 ^a	
		Flt-1	2.8 ^a	67 ^a	
		ZAP	>10 ^a	>240 ^a	
		EGFR	>20 ^a	>480 ^a	
		FGFR1	6.7 ^a	160 ^a	
		PDGFRβ	5.0 ^a	120 ^a	

^a These data are based on racemic **1**.

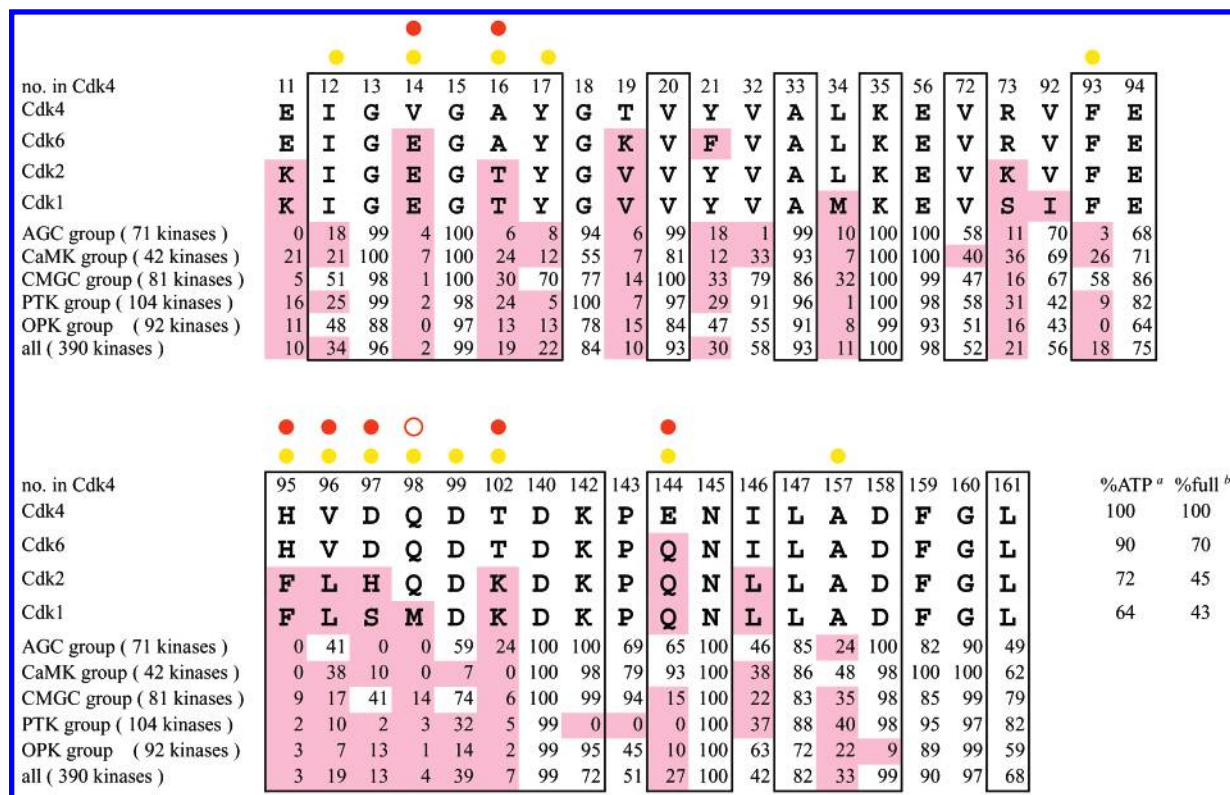


Figure 2. Amino acid residues around the ATP binding pocket. Numbers in rows of AGC-OPK groups and 390 kinases show conserved ratios. Red cells: residues that are replaced in Cdk1/2/6 or <40% conserved in 390 kinases. Box: residues in contact with or accessible to ATP γ S or compound **1**. Yellow circles: residues that are <40% conserved and are in contact with or are accessible to either ATP γ S or compound **1**. Red circles: residues that are replaced in both Cdk1 and Cdk2 and are in contact with or accessible to either ATP γ S or compound **1**. Red open circle: residues that are replaced in Cdk1 and are in contact with or accessible to either ATP γ S or compound **1**. ^aSequence identity confined to around the ATP binding pocket of Cdk4. ^bSequence identity based on full sequences.

The multiple alignment of 390 representative kinase sequences by S. K. Hanks and A. M. Quinn was published on the Internet.¹⁴ Using the multiple alignment, we calculated (1) the conserved ratios for each of the 39 residues of Cdk4 in the 390 kinases and (2) the amino acid identities in the region confined to the 39 residues around the ATP binding pocket. The multiple alignment among Cdk4, Cdk6, Cdk1, and Cdk2 and the results of the calculations are summarized in Figure 2. From these data, we were able to identify frequently altered amino acid residues in the 390 kinases and altered amino acid residues in Cdk1/2. Among the frequently altered residues, those with side chains not facing inhibitors are not useful for the design of new inhibitors. We must use the differences of chemical properties and/or shape of the residues' side chains that faced compound **1** to improve Cdk4 selectivity. For this purpose, 26 residues that were directly in contact with or accessible to ATP γ S or compound **1** were selected by considering the 3D structures of the complexes. These residues are enclosed in the boxes in Figure 2. Thirteen residues (Ile12, Val14, Ala16, Tyr17, Phe93, His95, Val96, Asp97, Gln98, Asp99, Thr102, Glu144, and Ala157), which are <40% conserved in 390 kinases and in contact with or accessible to ATP γ S or compound **1**, are shown by yellow circles in Figure 2. Among the 13 residues, Ile12, Tyr17, Phe93, and Asp99 are highly conserved in the CMGC group (Hanks' classification of kinases¹³), which includes Cdk4. Tyr17 is thought to be involved in regulation of

phosphorylation activity of the Cdk4 and related kinases.¹⁵ The side chains of Phe93, His95, Val96, and Ala157 were already predicted to have contact with compound **1** from X-ray analysis of the Cdk2-**1** complex. The moderately higher selectivity of compound **1** for Cdk4 over other kinases is likely to be due to specific interactions with these residues.

Subsequently, we tried to identify altered amino acid residues in Cdk4 and Cdk1/2. In the region of the ATP binding pocket of Cdk4, residue identities were found to be very high with respect to Cdk1/2 (64%/72%), while the identities throughout the full sequence were not as high (43%/45%). Among the residues around the ATP binding pocket, we identified eight residues (Val14, Ala16, His95, Val96, Asp97, Gln98, Thr102, and Glu144) which are altered in Cdk1/2 and have contact or are accessible to ATP γ S or compound **1** (these residues are shown by red circles and a red open circle in Figure 2). Except for Gln98, all of these residues are altered in both Cdk1 and Cdk2. Interestingly, Gln98 is conserved in Cdk2 as shown in Figure 3C. It is noteworthy that five of eight residues are distributed on one side of the ATP binding pocket. According to X-ray analyses of Cdk6-p16/p19 complexes, this side is the p16 binding region (Figure 3B).¹⁶ p16 is a Cdk4/6-specific, endogenous inhibitor protein that is thought to suppress carcinogenesis.¹⁷ Therefore, the amino acid residues in the p16 binding region of Cdk4 are likely to interact with p16 in a specific way.

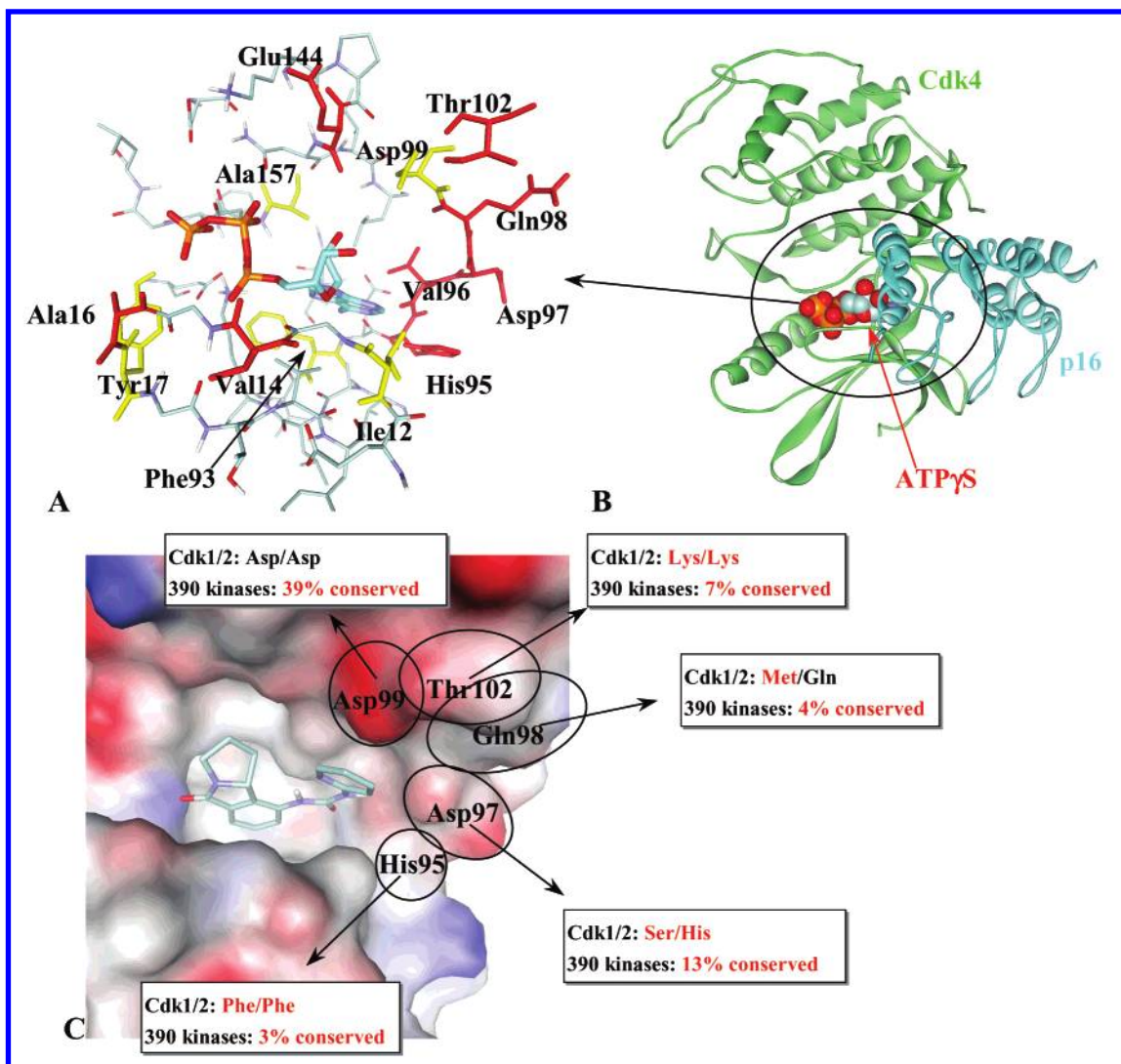


Figure 3. Locations of altered residues and the binding mode of **1**. A: locations of altered/frequently altered residues around the ATP binding pocket of Cdk4. Yellow residues: residues that are <40% conserved in 390 kinases and are in contact with or accessible to either ATP γ S or compound **1**. Red residues: residues that are replaced in Cdk1 or Cdk2, <40% conserved in 390 kinases, and are in contact with or accessible to either ATP γ S or compound **1**. B: superimposed model of the Cdk4–ATP γ S–p16 complex. Green ribbon: Cdk4 model. Cyan ribbon: p16. CPK representation: ATP γ S. The location of ATP γ S and p16 were predicted by superposition of the Cdk4 homology model, Thr160 phosphorylated Cdk2–cyclinA–ATP γ S (PDB ID: 1JST), and Cdk6–p16 (PDB ID: 1BI7). C: the binding mode of compound **1** in the Cdk4 homology model and altered/frequently altered residues in the p16 binding region. The Cdk4 homology model: solvent accessible surface (probe: 1.4 Å) representation (colored by partial charge). Compound **1**: stick representation.

By analyzing the binding mode of compound **1**, we found that the pyridine ring of compound **1** is directed toward the amino acid residues in the p16 binding region (Figure 3C). The terminal of the side chain of Val96 cannot come in contact with the inhibitor because it is hidden by the side chain of Leu147. Ile12 is replaced by Leu in most kinases, including Cdk1/2; this causes only small changes in the protein surface. For these reasons, we removed Val96 and Ile12 from target residues. On the other hand, Asp97 is replaced by His (Cdk2) or Ser (Cdk1), and Thr102 is replaced by Lys (Cdk1/2). These alterations cause dramatic changes of the chemical properties and shape of the protein surface. Amino acid residues such as Asp99, Gln98, and His95 are also useful. Asp99 is replaced by Ala, Ser, Asn, Pro, or Cys in most tyrosine kinases. Gln98 is replaced by Met in Cdk1 and by various other residues in other kinases. His95 is replaced by Phe in Cdk1/2 and by Phe or Tyr in most kinases. In this regard, in order to

enhance Cdk4 selectivity against Cdk1/2 and other kinases, the introduction of substituents that face the side chains of these residues was expected to be effective.

Library Design Based on Structural Information. To select first target residues to interact with substituents on our lead compounds, we calculated the shortest distances between the substitutable positions of the inhibitors and the side chain of each residue in the p16 binding region (Figure 4B). We found that compounds **2a** and **2b**, which have a five-membered pyrazole ring, are useful as leads in addition to compound **1** in order to approach these residues from various directions. The structures and inhibitory activities for Cdk4 of **2a** and **2b** are shown in Figure 4A, and the binding mode of **2a** predicted by a docking study is shown in Figure 4B. Asp99, Thr102, and Gln98 were more accessible than the other residues. On the basis of the binding modes, the 5-position of the pyrazole ring

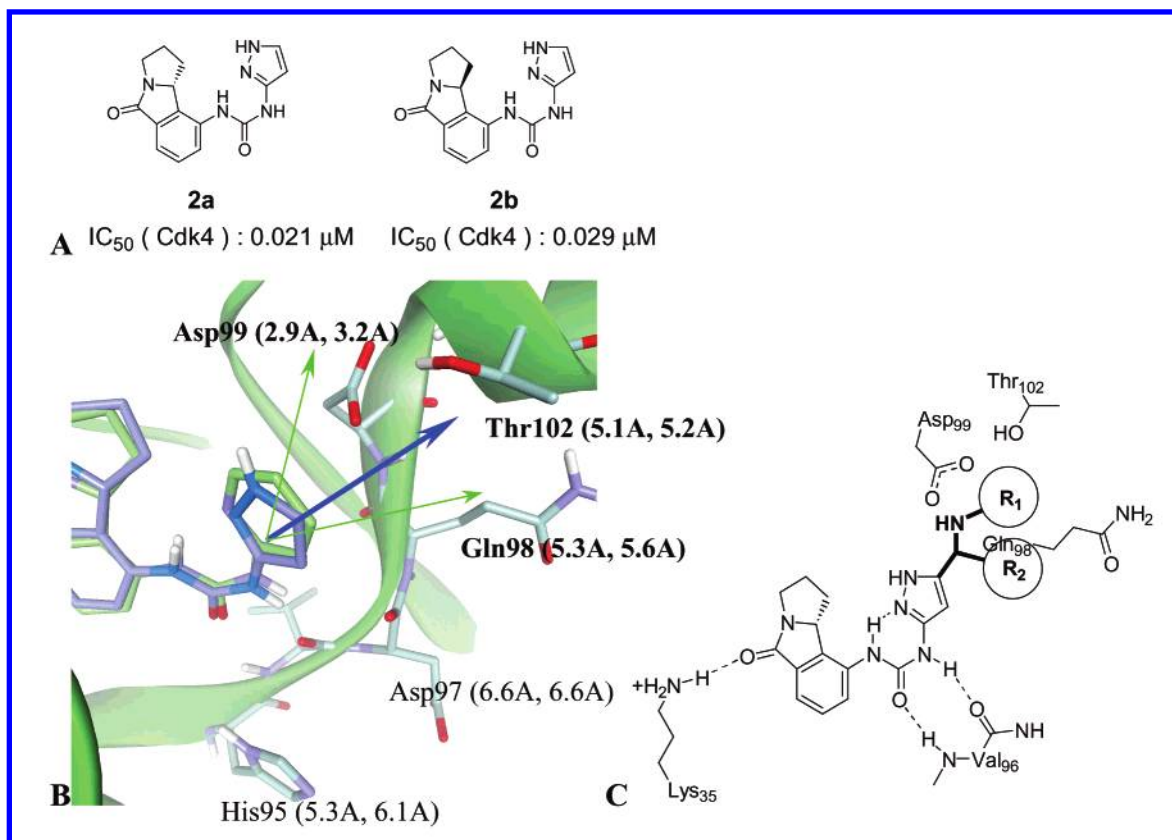


Figure 4. Predicted suitable substitution positions and substituents. A: structures of **2a** and **2b** and their IC_{50} (Cdk4) values. B: predicted binding modes of compound **1/2a** and suitable positions to introduce substituents. Green stick: compound **1**. Blue stick: compound **2a**. Left numbers: shortest distances between substitutable positions of the pyridine ring in compound **1** and the side chain of each residue. Right numbers: shortest distances between substitutable positions of the pyrazole ring in compound **2a** and the side chain of each residue. Arrows: directions of substituents on the pyridine ring and pyrazole ring. Bold arrow: predicted most appropriate direction toward Asp99, Thr102, and Glu98. C: schematic figure of binding mode of compound **2a** and appropriate substituent candidates. Bold line: a typical output structure interacted with Asp99, Thr102, and Glu98 that was proposed by *de novo* design programs (LUDI and LeapFrog).

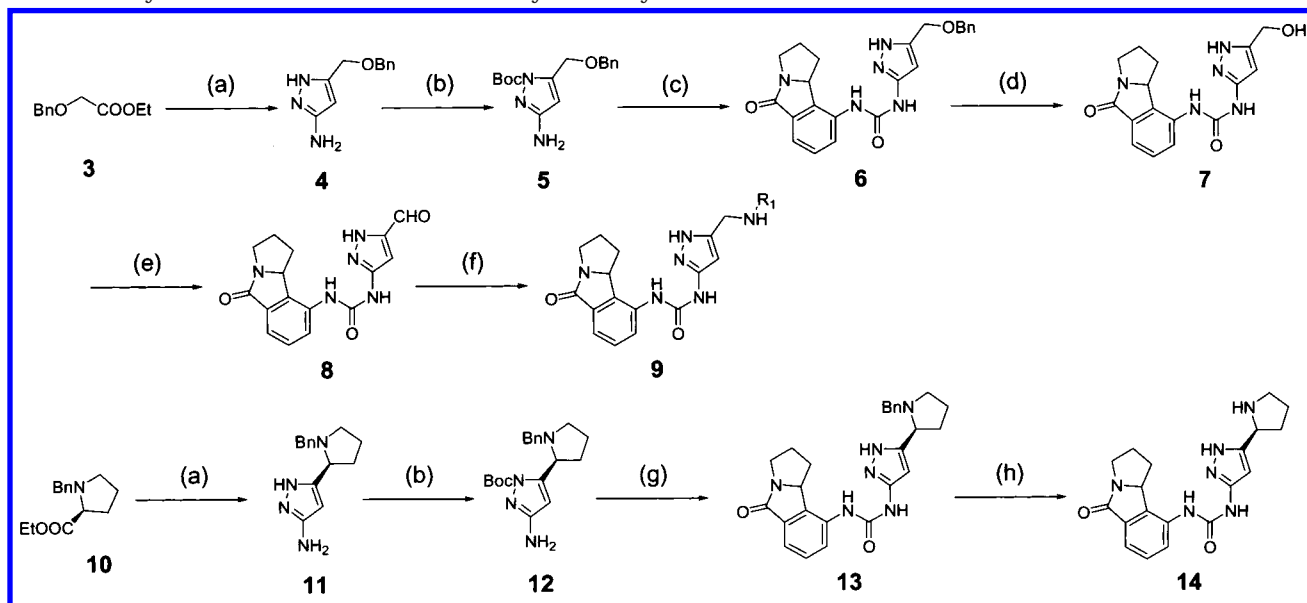
in compound **2a** (blue bold arrow in Figure 4B) was predicted to be the most appropriate position and direction to contact with the side chains of the three residues. Therefore, we constructed a 5-substituted pyrazol-3-yl urea library to enhance Cdk4 selectivity.

To design suitable substituents, we employed the *de novo* design programs,¹⁸ LUDI¹⁹ and LeapFrog.²⁰ Although output structures from *de novo* design programs are often not synthetically feasible, these structures suggest suitable properties such as a hydrogen-bonding donor, acceptor, and hydrophobicity and appropriate lengths of substituents. The aminomethyl groups and their cyclized groups were provided as typical structures by both LUDI and LeapFrog (Figure 4C). The NHs of these amino groups were predicted to interact with the carboxyl group of Asp99 and/or the side chain OH of Thr102. The OH of Thr usually functions as both a hydrogen-bonding donor and acceptor. However, in this case, the OH of Thr102 was already predicted to make a hydrogen bond with the carboxyl group of Asp99, and the side chain of Thr102 was expected to work as a hydrogen-bonding acceptor and hydrophobic portion for our lead compounds. As alkyl groups via the aminomethyl group, hydrophobic substituents were thought to be appropriate considering the hydrophobic environment surrounded by the side chain methyl group of Thr102 and the side chain methylene group of Gln98. These alkylamino groups can be easily introduced by

reductive amination with the corresponding aldehyde of compound **2a**. Thus we constructed a chemical library of **2a** featuring a pyrazole ring with alkylaminomethyl substituents at the 5-position.

The synthetic routes of alkylaminomethyl library **9** and the cyclized amino substituted compound **14** are summarized in Scheme 1. Compound **4** was prepared by the sequential coupling of **3**, acetonitrile, and hydrazine.²¹ Protection of **4** by the Boc group followed by a coupling reaction with 9-amino-1,2,3,9b-tetrahydro-5H-pyrrolo[2,1-*a*]isoindol-5-one⁶ provided the diarylurea compound **6** as a racemate. Deprotection and oxidation by MnO_2 gave aldehyde **8**, which was a substrate for reductive amination. The imine formation of **8** by treatment with alkylamines and $MS3\text{\AA}$ followed by a reduction provided the alkylamino library **9**. Synthesis of the cyclized amino substituted compound **14** was initiated from the optically active (*S*)-proline derivative. The diarylurea compound **13** was prepared by a procedure similar to that for synthesis of **6**. Deprotection of **13** gave compound **14**.

SAR Profiles and Structural Basis for Selective Cdk4 Inhibition. Compounds in the first alkylamino library (64 compounds) were tested by both cyclin D-Cdk4 and cyclin A-Cdk2 inhibitory assay. The potencies and Cdk4 selectivities over Cdk2 of the representative compounds are summarized in Table 2. Interestingly, introduction of the amino groups caused

Scheme 1. Synthetic Routes of 5-Substituted Pyrazole-3-yl Urea Derivatives^a

^a Reagents: (a) (1) BuLi, CH₃CN, tetrahydrofuran; (2) NH₂NH₂, EtOH, 40% (for **4**), 81% (for **11**); (b) NaH, (Boc)₂O, tetrahydrofuran, 53% (for **5**), 61% (for **12**); (c) (1) 4-(dimethylamino)pyridine, *p*-nitrophenyl chloroformate, CHCl₃; (2) amine;²⁵ (3) 4 N HCl, MeOH, 19%; (d) Pd(OH)₂/C, H₂, 2 N HCl, MeOH–tetrahydrofuran, 93%; (e) MnO₂, CHCl₃–dimethylformamide, 59%; (f) (1) alkylamine, MS3A, chloroform–MeOH; (2) NaBH₄, 20–50%; (g) (1) NaH, 4-nitrophenyl chloroformate, tetrahydrofuran; (2) amine;²⁵ 4-(dimethylamino)pyridine, 42%; (3) 6 N HCl, MeOH, 21%; (h) Pd/C, H₂, 4 N HCl, MeOH, 51%.

Table 2. IC₅₀ Values and Cdk4 Selectivity over Cdk2 of 5-Alkylaminomethyl-pyrazole-3-yl Urea Derivatives

no.	R	Inhibitory activity (IC ₅₀ , μM)		Selectivity (-fold)
		D-Cdk4	A-Cdk2	
9a		0.29	14	48
9b		0.16	12	75
9c		0.13	17	130
9d		0.056	9.8	180
9e		0.065	9.7	150
9f		0.72	20	27
9g		0.47	7.5	16
9h		0.25	12	48

a 100–200-fold decrease in Cdk2 inhibitory activity as compared to that of compound **1** (IC₅₀ (Cdk2) = 0.078 μM). Although addition of these amino groups also

caused reduction of Cdk4 inhibitory activity in general, the compounds substituted with *tert*-butyl (**9d**) and cyclopentyl (**9e**) had almost comparable inhibition potencies to that of compound **1**. Consequently, **9d** and **9e** showed better Cdk4 selectivities over Cdk2 (180-fold and 150-fold, respectively). These SARs and structural information around the p16 binding region suggested that (1) NH₂⁺s on the alkylamino groups formed a hydrogen bond with the carboxyl group of Asp99 (Asp86 in Cdk2), (2) in Cdk2, the alkylamino groups constrained by the hydrogen bond with Asp86, caused electrostatic and/or steric repulsion with the side chain of Lys89, and (3) in Cdk4, the hydrophobic and bulky substituents of **9d** and **9e** fit into the hydrophobic region surrounded by the side chains of Thr102 and Gln98.

From these facts, we designed **14a** and **14b** with a pyrrolidine ring to restrict the substituent, and **15a** and **15b** with a 5-chloroindan-2-ylaminomethyl group to enhance the hydrophobic interaction with Cdk4, while maintaining selectivity over Cdk2. Each compound was prepared as a single diastereomer²² by chiral HPLC separation. The potency and Cdk4 selectivity over Cdk1/2 of each compound are summarized in Table 3. Compound **14a** and **14b** showed comparable selectivities over Cdk2 (110-fold/120-fold) to that of **9d** and **9e**. We successfully completed X-ray analysis of the mutant Cdk2 (Cdk4 mimic Cdk2, having F82H, L83V, and K89T)–**14b** complex (PDB ID: 1GLJ) using the soaking method (Figure 5A).⁹ In this X-ray structure, the NH₂⁺ group of pyrrolidine in **14b** formed a salt bridge with the carboxyl group of Asp86, which proved our hypothesis. On the other hand, **15a/15b** showed 30–40-fold enhancement of Cdk4 inhibitory activity (0.0016 μM/0.0023 μM) compared to that of **9e** with good selectivity over Cdk2. The docking studies²³ between Cdk4/Cdk2 and **15b** predicted steric repulsion between the large chloroindanyl group constrained by the hydrogen bond

Table 3. IC₅₀ Values and Cdk4 Selectivity over Cdk1/2 of Designed Compounds

no.	R ₁	R ₂	Inhibitory activity (IC ₅₀ , μM)			Selectivity (-fold)	
			D-Cdk4	A-Cdk2	B-Cdk1	Cdk2/Cdk4	Cdk1/Cdk4
			14a			0.22	25
14b			0.21	25	28	120	130
15a			0.0016	0.18	0.54	110	340
15b			0.0023	0.44	1.80	190	780

with Asp86 and the side chain of Lys89 in Cdk2 (Figure 5C). In addition, it was predicted that the chloroindanyl group in **15b** will make good van der Waals contact with the side chains of Thr102 and Gln98 in the Cdk4 model. This contact between hydrophobic surfaces possibly contributes to the enhanced binding affinity of **15b** with Cdk4. Interestingly, **15b** showed higher selectivity over Cdk1 (780-fold) than over Cdk2 (190-fold), while **14a** showed almost equal selectivity over both Cdk1 (130-fold) and Cdk2 (120-fold). As already shown in Figure 3C, Gln98 in Cdk4 is replaced by Met in Cdk1 but is conserved in Cdk2. This difference between Cdk1 and Cdk2 may cause different inhibitory activities between Cdk1 (0.44 μM) and Cdk2 (1.8 μM).

Finally, we investigated the Cdk4 selectivity of **15b** over other representative kinases. Schematic figures of the binding modes of the key compounds **1** and **15b**, their Cdk4 selectivity over representative kinases, and the sequence alignment (Asp99, Thr102, and Gln98) are summarized in Figure 6. The selectivity of **15b** over Cdk1/2 was remarkably higher than that of compound **1**, while the selectivity of **15b** over other Ser/Thr kinases and Tyr kinases remained the same or were enhanced. The NH₂⁺ of **15b**, which is assumed to interact with Asp99, is critical for the higher Cdk4 selectivity not only over Cdk1/2 but also over other kinases. As shown in Figure 6, this Asp99 is replaced by the nonacidic residues in most tyrosine kinases. Thr102 and Gln98 are also frequently replaced by other residues in both Ser/Thr kinases and tyrosine kinases. The interactions between the three residues and **15b** were supposed to contribute to the improvement in Cdk4 selectivity over Lck (3000-fold), Flt-1 (480-fold), FGFR1 (7000-fold), and PDGFRβ (1500-fold) compared with those of compound **1**.

Conclusion

We developed a highly selective and potent Cdk4 inhibitor **15b** by structure-based drug design. Compound **15b** showed excellent selectivity not only over Cdk1/2 (780-fold/190-fold) but also over many other kinases (>430-fold) so far investigated. Cell-based studies revealed that **15b** of between 0.1 and 0.5 μM concentration causes G₁ arrest in the Rb(+) cancer cell line (Molt-4). Further details regarding the cellular profiles of these Cdk4 selective inhibitors will be reported in a following manuscript.²³

Identification of altered residues in Cdk1/2 and in 390 other kinases in their ATP binding pockets allowed us to focus on target residues to interact with substituents on lead compounds. Library design based on the locations of these residues and the binding modes of lead compounds enabled us to develop potent and selective compounds efficiently.

The kinase superfamily consists of numerous kinases that have a common folding pattern. Therefore, in general it is difficult to improve target kinase selectivity with respect to all the other kinases at the same time. Our approach should be helpful for the development of specific kinase inhibitors more systematically and efficiently.

Experimental Section

Materials and Methods. All reagents and solvents were of commercial quality and were used without further purification unless otherwise noted. Melting points were determined with a Yanaco MP micromelting point apparatus (Yanagimoto Seisakusho Co., Ltd., Japan) and were not corrected. ¹H NMR spectra were obtained on a Varian Gemini-300 (300 MHz) or Gemini-200 (200 MHz) with tetramethylsilane as an internal standard. Mass spectrometry was performed with a JEOL JMS-SX 102A (FAB positive) or micromass QUATTRO II (ESI positive). High-resolution mass spectra (HR-MS) were deter-

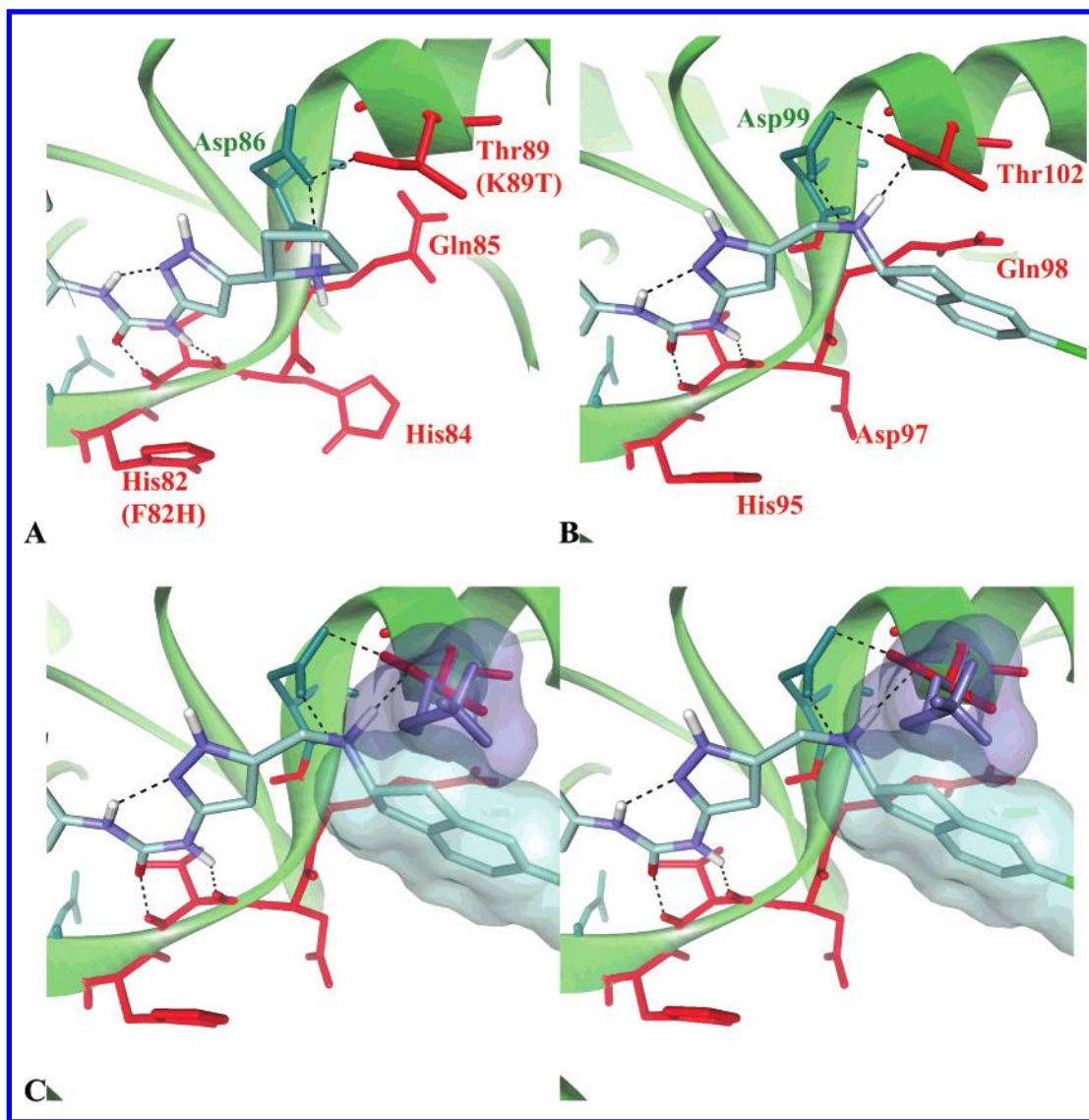


Figure 5. Structural basis of selective Cdk4 inhibition by compound **15b**. A: binding mode of **14b** in Cdk4 mimic Cdk2 (X-ray, PDB ID: 1GIJ). ⁹ B: binding mode of **15b** in Cdk4 (model). C: steric repulsion between chloroindane in **15b** and the side chain of Lys89 (stereoview). Dark blue stick: the side chain of Lys89, whose conformation originated from X-ray analysis of Thr160 phosphorylated Cdk2-cyclin A-ATP γ S complex (PDB ID: 1JST). The location of Lys89 was determined by superposition of the Cdk4 homology model and 1JST. Cyan cloud: van der Waals surface representation of chloroindane. Dark blue cloud: van der Waals surface representation of Lys89 in Cdk2.

mined with a micromass Q-TOF2 (ESI positive). Optical rotations were measured with a Jasco DIP-370 polarimeter. Thin-layer chromatography (TLC) analysis was performed on Merck Kieselgel F₂₅₄ precoated plates. Silica gel column chromatography was carried out on Wako gel C-300 (Wako Pure Chemicals Industries, Ltd., Japan).

***N*-[(9*bR*)-5-Oxo-2,3,5,9*b*-tetrahydro-1*H*-pyrrolo[2,1-*a*]-isoindol-9-yl]-*N*-(1*H*-pyrazol-3-yl)urea (**2a**).** To a stirred solution of 1-benzyl-3-aminopyrazole²⁴ (150 mg, 0.74 mmol) in CHCl₃ (10 mL) were added 4-(dimethylamino)pyridine (139 mg, 1.63 mmol) and 4-nitrophenyl chloroformate (143 mg, 0.74 mmol). After the solution was stirred for 30 min at 70 °C, (9*bR*)-9-amino-1,2,3,9*b*-tetrahydro-5*H*-pyrrolo[2,1-*a*]-isoindol-5-one⁶ (70 mg, 0.37 mmol) was added, and the reaction mixture was stirred for 10 h at the same temperature. The solvent was removed in vacuo, and the residue was purified by silica gel column chromatography (3% MeOH in CHCl₃) to give crude *N*-(1-benzyl-1*H*-pyrazol-3-yl)-*N*-[(9*bR*)-5-oxo-2,3,5,9*b*-tetrahydro-1*H*-pyrrolo[2,1-*a*]-isoindol-9-yl]urea (136 mg). The solution of crude *N*-(1-benzyl-1*H*-pyrazol-3-yl)-*N*-[(9*bR*)-5-oxo-2,3,5,9*b*-tetrahydro-1*H*-pyrrolo[2,1-*a*]-isoindol-9-yl]urea (136 mg) in MeOH-tetrahydrofuran (1:1) was mixed with palladium hydroxide (on carbon, 100 mg) and 2 N HCl (100 μ L).

The mixture was stirred for 10 h at 50 °C under an atmospheric pressure of hydrogen. The catalyst was removed by filtration and concentrated in vacuo. The residue was purified by silica gel column chromatography (3% MeOH in CHCl₃) and recrystallized from EtOAc to yield **2a** (58 mg, 53%, two steps) as a white solid. mp 248–249 °C. ¹H NMR (300 MHz, DMSO-*d*₆): δ 1.02–1.09 (1H, m), 2.26–2.37 (2H, m), 2.59–2.64 (1H, m), 3.26–3.33 (1H, m), 3.52–3.56 (1H, m), 4.70 (1H, dd, $J_1 = 10.4$ Hz, $J_2 = 5.7$ Hz), 6.14 (1H, brs), 7.27 (1H, d, $J = 8.0$ Hz), 7.43 (1H, t, $J = 8.0$ Hz), 7.64 (1H, s), 8.25 (1H, d, $J = 8.0$ Hz), 8.40–9.60 (1H, br), 9.47 (1H, s), 12.39 (1H, brs). MS (ESI⁺): m/z 298 (M+H)⁺. HR-MS calcd for C₁₅H₁₆N₅O₂ (M+H)⁺: 298.1304, found 298.1300. [α]_D²⁰ 115.8° (c 1.0, CHCl₃). Anal. (C₁₅H₁₅N₅O₂·0.1EtOAc) C, H, N.

***N*-[(9*bS*)-5-Oxo-2,3,5,9*b*-tetrahydro-1*H*-pyrrolo[2,1-*a*]-isoindol-9-yl]-*N*-(1*H*-pyrazol-3-yl)urea (**2b**).** To a stirred solution of 1-benzyl-3-aminopyrazole²⁴ (150 mg, 0.74 mmol) in CHCl₃ (10 mL) were added 4-(dimethylamino)pyridine (139 mg, 1.63 mmol) and 4-nitrophenyl chloroformate (143 mg, 0.74 mmol). After the solution was stirred for 30 min at 70 °C, (9*bS*)-9-amino-1,2,3,9*b*-tetrahydro-5*H*-pyrrolo[2,1-*a*]-isoindol-5-one⁶ (70 mg, 0.37 mmol) was added, and the reaction mixture was stirred for 10 h at the same temperature. The

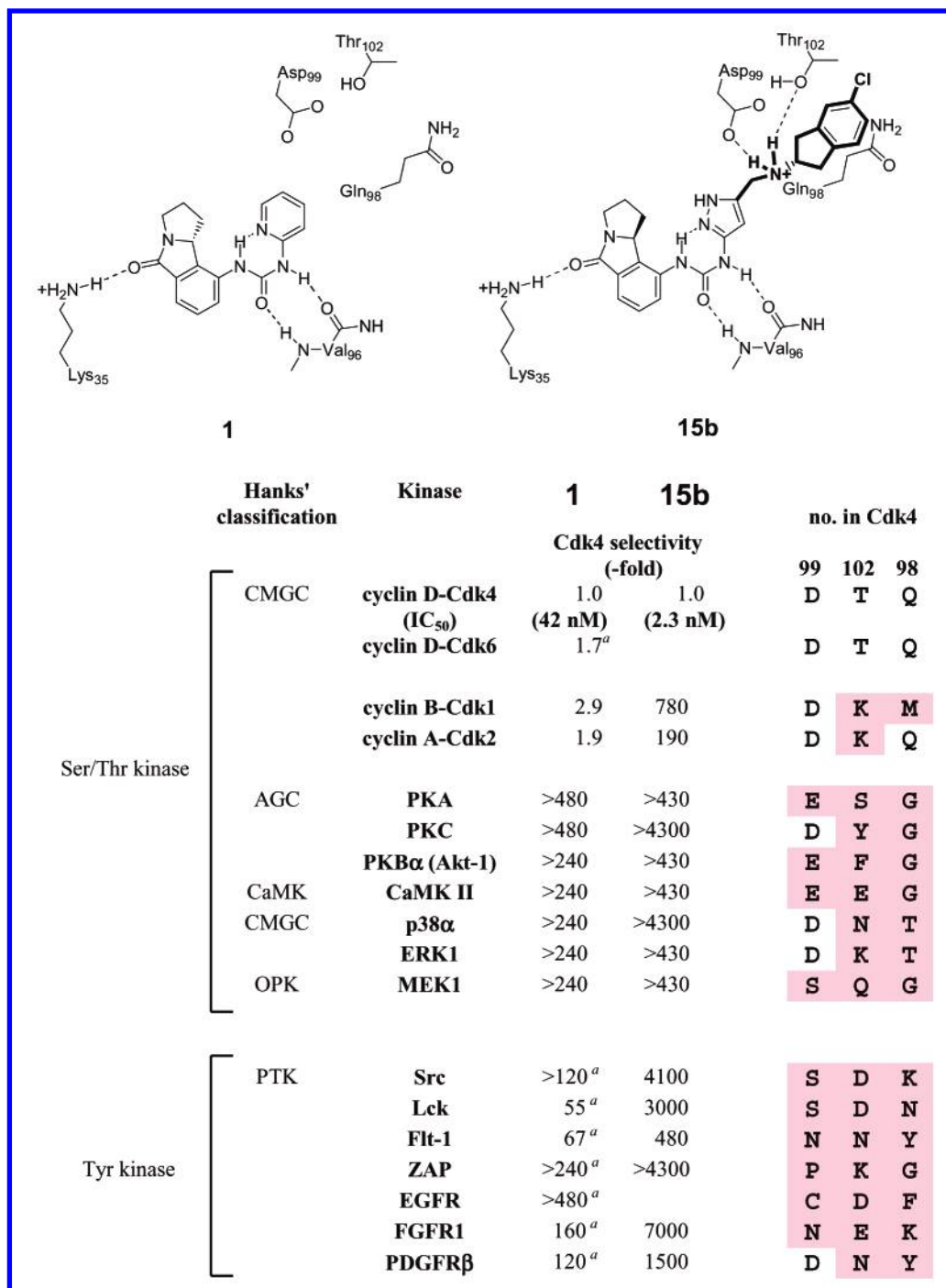


Figure 6. Cdk4 selectivity of key compounds **1** and **15b** over Cdk1/2 and other representative kinases, and sequence alignment (Asp99, Thr102, and Gln98).

solvent was removed in vacuo, and the residue was purified by silica gel column chromatography (3% MeOH in CHCl₃) to give crude *N*-(1-benzyl-1*H*-pyrazol-3-yl)-*N'*-[(9*b*.*S*)-5-oxo-2,3,5,9*b*-tetrahydro-1*H*-pyrrolo[2,1-*a*]isoindol-9-yl]urea (149 mg). The solution of crude *N*-(1-benzyl-1*H*-pyrazol-3-yl)-*N'*-[(9*b*.*S*)-5-oxo-2,3,5,9*b*-tetrahydro-1*H*-pyrrolo[2,1-*a*]isoindol-9-yl]urea (149 mg) in MeOH–tetrahydrofuran (1:1) was mixed with palladium hydroxide (on carbon, 100 mg) and 2 N HCl (100 μL). The mixture was stirred for 10 h at 50 °C under an atmospheric pressure of hydrogen. The catalyst was removed by filtration and concentrated in vacuo. The residue was purified by silica gel column chromatography (3% MeOH in CHCl₃) and recrystallized from EtOAc to yield **2b** (63 mg, 57%, two steps) as a white solid. mp 248–249 °C. ¹H NMR (300 MHz, DMSO-*d*₆): δ 1.02–1.09 (1H, m), 2.26–2.37 (2H, m), 2.59–2.64 (1H, m), 3.26–3.33 (1H, m), 3.52–3.56 (1H, m), 4.70

(1H, dd, *J*₁ = 10.4 Hz, *J*₂ = 5.7 Hz), 6.14 (1H, brs), 7.27 (1H, d, *J* = 8.0 Hz), 7.43 (1H, t, *J* = 8.0 Hz), 7.64 (1H, s), 8.25 (1H, d, *J* = 8.0 Hz), 8.40–9.60 (1H, br), 9.47 (1H, s), 12.39 (1H, brs). MS (ESI⁺): *m/z* 298 (M+H)⁺. HR-MS calcd for C₁₅H₁₆N₅O₂ (M+H)⁺: 298.1304, found 298.1304. [α]_D²⁰ –115.4° (*c* 1.0, CHCl₃). Anal. (C₁₅H₁₅N₅O₂·0.1EtOAc) C, H, N.

5-[(Benzyloxy)methyl]-1*H*-pyrazol-3-amine (4). To a stirred solution of acetonitrile (10.2 mL, 195 mmol) in tetrahydrofuran (500 mL) was added butyllithium (130 mL, 1.5 M solution of hexane, 196 mmol) at –78 °C. After the solution was stirred for 30 min at the same temperature, ethyl benzyloxyacetate (**3**)²⁵ (34.0 g, 178 mmol) was added. The reaction mixture was stirred at room temperature for 2 h and then poured into water. The solution was acidified with 1 N HCl and extracted with EtOAc. The organic layer was concentrated in vacuo. A solution of the residue (17.3 g) in ethanol (200 mL)

was mixed with hydrazine monohydrate (26 mL, 536 mmol) and refluxed for 10 h. The reaction mixture was evaporated in vacuo, and the residue was diluted with CHCl₃ and washed with brine. The organic layer was concentrated in vacuo, and the residue was purified by silica gel column chromatography (2% MeOH in CHCl₃) to give **4** (14.5 g, 40%, two steps). ¹H NMR (200 MHz, CDCl₃): δ 3.48 (2H, s), 4.47 (2H, s), 4.53 (2H, s), 5.58 (1H, s), 7.20–7.44 (6H, m). MS (ESI⁺): *m/z* 204 (M+H)⁺.

tert-Butyl 3-Amino-5-[(benzyloxy)methyl]-1H-pyrazole-1-carboxylate (5). To a stirred solution of **4** (14.5 g, 71.3 mmol) in tetrahydrofuran–dimethylformamide (3:2, 250 mL) was added sodium hydride (3.1 g, 60 wt % in mineral oil, 78.4 mmol) at 0 °C. After the solution was stirred for 30 min, di-*tert*-butyl dicarbonate (17.1 g, 78.4 mmol) was added. The resultant mixture was stirred for 2 h at room temperature, poured into saturated aqueous NH₄Cl, and extracted with CHCl₃. The organic layer was washed with brine, dried over MgSO₄, and concentrated in vacuo. The residue was purified by silica gel column chromatography (2% MeOH in CHCl₃) to yield **5** (11.5 g, 53%). ¹H NMR (300 MHz, CDCl₃): δ 1.68 (9H, s), 3.49 (1H, d, *J* = 5.6 Hz), 4.52 (2H, s), 4.58 (2H, s), 5.34 (2H, br), 5.54 (1H, s), 7.28–7.40 (5H, m). MS (ESI⁺): *m/z* 304 (M+H)⁺.

N-{5-[(Benzyloxy)methyl]-1H-pyrazol-3-yl}-N'-(5-oxo-2,3,5,9b-tetrahydro-1H-pyrrolo[2,1-*a*]isoindol-9-yl)urea (6). To a stirred solution of **5** (5.0 g, 16 mmol) in CHCl₃ (50 mL) were added 4-(dimethylamino)pyridine (2.2 g, 18 mmol) and 4-nitrophenyl chloroformate (3.65 g, 17 mmol). After the solution was stirred for 30 min at 70 °C, 9-amino-1,2,3,9b-tetrahydro-5H-pyrrolo[2,1-*a*]isoindol-5-one⁶ (3.4 g, 17 mmol) was added. The reaction mixture was stirred for 2 h at the same temperature. The solvent was removed in vacuo, and the residue was purified by silica gel column chromatography (2% MeOH in CHCl₃) to give crude *tert*-butyl 5-[(benzyloxy)methyl]-3-({[(5-oxo-2,3,5,9b-tetrahydro-1H-pyrrolo[2,1-*a*]isoindol-9-yl)-amino]carbonyl}amino)-1H-pyrazole-1-carboxylate (2.5 g). A solution of crude *tert*-butyl 5-[(benzyloxy)methyl]-3-({[(5-oxo-2,3,5,9b-tetrahydro-1H-pyrrolo[2,1-*a*]isoindol-9-yl)-amino]carbonyl}amino)-1H-pyrazole-1-carboxylate (2.5 g) in MeOH was mixed with 4 N HCl (5 mL, dioxane solution). After the solution was stirred for 30 min at room temperature, the reaction mixture was diluted with CHCl₃, and the organic layer was washed with brine, dried over MgSO₄, and concentrated in vacuo. The residue was purified by silica gel column chromatography (5% MeOH in CHCl₃) to yield **6** (1.3 g, 19%, two steps) as a white solid. ¹H NMR (300 MHz, DMSO-*d*₆): δ 1.01–1.10 (1H, m), 2.28–2.33 (2H, m), 2.59–2.65 (1H, m), 3.25–3.31 (1H, m), 3.51 (1H, d, *J* = 8.2 Hz), 4.50 (2H, s), 4.70 (1H, dd, *J*₁ = 10.5 Hz, *J*₂ = 5.9 Hz), 6.15 (1H, brs), 7.26–7.46 (8H, m), 8.25 (1H, d, *J* = 8.2 Hz), 9.46 (1H, s), 12.50 (1H, brs). MS (ESI⁺): *m/z* 418 (M+H)⁺.

N-[5-(Hydroxymethyl)-1H-pyrazol-3-yl]-N'-(5-oxo-2,3,5,9b-tetrahydro-1H-pyrrolo[2,1-*a*]isoindol-9-yl)urea (7). To a stirred solution of **6** (1.3 g, 3.1 mmol) in MeOH–tetrahydrofuran (1:1, 100 mL) were added palladium hydroxide (on carbon, 500 mg) and 2 N HCl (1.0 mL), and the mixture was stirred for 10 h at 50 °C under an atmospheric pressure of hydrogen. The catalyst was removed by filtration and concentrated in vacuo. The residue was precipitated from EtOAc–hexane to yield **7** (0.94 g, 93%) as a white solid. ¹H NMR (300 MHz, DMSO-*d*₆): δ 1.01–1.08 (1H, m), 2.30–2.33 (2H, m), 2.63–2.66 (1H, m), 3.16 (1H, d, *J* = 5.2 Hz), 3.47–3.53 (1H, m), 4.64 (2H, d, *J* = 5.6 Hz), 4.70 (1H, dd, *J*₁ = 10.3 Hz, *J*₂ = 5.7 Hz), 5.30 (1H, d, *J* = 5.4 Hz), 6.02 (1H, brs), 7.26 (1H, d, *J* = 6.6 Hz), 7.43 (1H, t, *J* = 6.6 Hz), 8.27 (1H, d, *J* = 6.6 Hz), 9.44 (1H, s), 12.30 (1H, brs). MS (ESI⁺): *m/z* 328 (M+H)⁺.

N-(5-Formyl-1H-pyrazol-3-yl)-N'-(5-oxo-2,3,5,9b-tetrahydro-1H-pyrrolo[2,1-*a*]isoindol-9-yl)urea (8). To a stirred solution of **7** (0.94 g, 2.9 mmol) in CHCl₃–dimethylformamide (1:2, 15 mL) was added MnO₂ (1.5 g, 17.3 mmol). After the solution was stirred for 1 h at 50 °C, the reaction mixture was filtered. The filtrate was concentrated in vacuo, and the residue was purified by silica gel column chromatography (10%

MeOH in CHCl₃) to yield **8** (0.56 g, 59%) as a white solid. mp 230 °C, dec ¹H NMR (300 MHz, DMSO-*d*₆): δ 0.98–1.09 (1H, m), 2.25–2.36 (2H, m), 2.48–3.36 (2H, m), 3.49–3.53 (1H, m), 4.74 (1H, dd, *J*₁ = 10.4 Hz, *J*₂ = 5.7 Hz), 7.14 (1H, s), 7.32 (1H, d, *J* = 8.0 Hz), 7.46 (1H, t, *J* = 8.0 Hz), 8.14 (1H, d, *J* = 8.0 Hz), 8.42 (1H, brs), 9.68 (1H, br), 9.79 (1H, brs), 10.26 (1H, s). MS (ESI⁺): *m/z* 326 (M+H)⁺. HR-MS calcd for C₁₆H₁₆N₅O₃ (M+H)⁺: 326.1253, found 326.1262.

General Procedure for Preparation of Alkylaminomethyl Library (9). To a stirred solution of **8** (30 mg, 0.092 mmol) and MS3Å (30 mg) in MeOH (3 mL) was added 3.0 equiv of amine at room temperature. After the solution was stirred for 12 h at the same temperature, NaBH₄ (100 mg, 2.64 mmol) was added. The resultant mixture was stirred for 1 h, poured into 1 N HCl, neutralized with saturated aqueous NaHCO₃, and extracted with CHCl₃. The organic layer was washed with brine, dried over MgSO₄, and concentrated in vacuo. The residue was purified by preparative silica gel chromatography (20% MeOH in CHCl₃) to yield **9**. Yields ranged from 20 to 50%.

The following compounds (**9a**, **9b**, **9c**, **9d**, **9e**, **9f**, **9g**, **9h**, **15a**, and **15b**) were prepared from the appropriate amines and **8** by the same procedure.

N-{5-[(Methylamino)methyl]-1H-pyrazol-3-yl}-N'-(5-oxo-2,3,5,9b-tetrahydro-1H-pyrrolo[2,1-*a*]isoindol-9-yl)urea (9a). ¹H NMR (300 MHz, DMSO-*d*₆): δ 0.95–1.10 (1H, m), 2.49 (3H, s), 2.20–2.80 (3H, m), 3.20–3.60 (2H, m), 4.12 (2H, m), 4.79 (1H, dd, *J*₁ = 10.2 Hz, *J*₂ = 5.3 Hz), 6.41 (1H, s), 7.29 (1H, d, *J* = 7.9 Hz), 7.44 (1H, t, *J* = 7.9 Hz), 8.21 (1H, d, *J* = 7.9 Hz), 9.12 (2H, br), 9.90 (1H, brs). MS (ESI⁺): *m/z* 341 (M+H)⁺. HR-MS calcd for C₁₇H₂₁N₆O₂ (M+H)⁺: 341.1726, found 341.1726.

N-(5-Oxo-2,3,5,9b-tetrahydro-1H-pyrrolo[2,1-*a*]isoindol-9-yl)-N'-(5-[(propylamino)methyl]-1H-pyrazol-3-yl)urea (9b). ¹H NMR (300 MHz, DMSO-*d*₆): δ 0.91 (1H, t, *J* = 7.5 Hz), 0.90–1.22 (1H, m), 1.60–1.75 (1H, m), 2.22–2.40 (2H, m), 2.65–2.77 (1H, m), 2.80–2.82 (2H, m), 3.25–3.35 (1H, m), 3.45–3.60 (1H, m), 4.13 (1H, m), 4.80 (1H, dd, *J*₁ = 10.4 Hz, *J*₂ = 5.9 Hz), 6.43 (1H, s), 7.28 (1H, d, *J* = 7.3 Hz), 7.44 (1H, t, *J* = 7.3 Hz), 8.21 (1H, d, *J* = 7.3 Hz), 9.23 (2H, br), 9.95 (1H, s). MS (ESI⁺): *m/z* 369 (M+H)⁺. HR-MS calcd for C₁₉H₂₅N₆O₂ (M+H)⁺: 369.2039, found 369.2036.

N-{5-[(Isopropylamino)methyl]-1H-pyrazol-3-yl}-N'-(5-oxo-2,3,5,9b-tetrahydro-1H-pyrrolo[2,1-*a*]isoindol-9-yl)urea (9c). ¹H NMR (300 MHz, DMSO-*d*₆): δ 0.91 (1H, t, *J* = 7.5 Hz), 0.98–1.15 (1H, m), 1.27 (6H, d, *J* = 6.4 Hz), 2.25–2.42 (2H, m), 2.40–2.60 (1H, m), 2.66–2.78 (1H, m), 3.25–3.42 (2H, m), 3.45–3.62 (1H, m), 4.13 (2H, m), 4.80 (1H, dd, *J*₁ = 10.4 Hz, *J*₂ = 5.9 Hz), 6.44 (1H, s), 7.43 (1H, d, *J* = 7.7 Hz), 8.20 (1H, d, *J* = 7.7 Hz), 9.15 (2H, br), 9.91 (1H, s). MS (ESI⁺): *m/z* 369 (M+H)⁺. HR-MS calcd for C₁₉H₂₅N₆O₂ (M+H)⁺: 369.2039, found 369.2039.

N-{5-[(*tert*-Butylamino)methyl]-1H-pyrazol-3-yl}-N'-(5-oxo-2,3,5,9b-tetrahydro-1H-pyrrolo[2,1-*a*]isoindol-9-yl)urea (9d). ¹H NMR (300 MHz, DMSO-*d*₆): δ 0.91 (1H, t, *J* = 7.5 Hz), 0.95–1.12 (1H, m), 1.35 (9H, s), 2.22–2.38 (2H, m), 2.62–2.75 (1H, m), 3.32–3.37 (1H, m), 3.42–3.60 (1H, m), 4.10 (2H, m), 4.79 (1H, dd, *J*₁ = 10.4 Hz, *J*₂ = 5.9 Hz), 6.47 (1H, s), 7.29 (1H, d, *J* = 7.3 Hz), 7.45 (1H, t, *J* = 7.3 Hz), 8.22 (1H, d, *J* = 7.3 Hz), 9.09 (2H, br), 9.91 (1H, s). MS (ESI⁺): *m/z* 383 (M+H)⁺. HR-MS calcd for C₂₀H₂₇N₆O₂ (M+H)⁺: 383.2195, found 383.2200.

N-{5-[(Cyclopentylamino)methyl]-1H-pyrazol-3-yl}-N'-(5-oxo-2,3,5,9b-tetrahydro-1H-pyrrolo[2,1-*a*]isoindol-9-yl)urea (9e). ¹H NMR (300 MHz, DMSO-*d*₆): δ 0.90–1.20 (1H, m), 1.20–2.00 (8H, m), 2.20–2.70 (4H, m), 3.00–3.40 (1H, m), 3.40–3.60 (1H, m), 3.74 (2H, m), 4.69 (1H, m), 7.25 (1H, d, *J* = 7.9 Hz), 7.41 (1H, t, *J* = 7.9 Hz), 8.21 (1H, d, *J* = 7.9 Hz), 9.44 (1H, br), 12.20 (1H, br). MS (ESI⁺): *m/z* 395 (M+H)⁺. HR-MS calcd for C₂₁H₂₇N₆O₂ (M+H)⁺: 395.2205, found 395.2205.

N-{5-[(Cyclohexylamino)methyl]-1H-pyrazol-3-yl}-N'-(5-oxo-2,3,5,9b-tetrahydro-1H-pyrrolo[2,1-*a*]isoindol-9-yl)urea (9f). ¹H NMR (300 MHz, DMSO-*d*₆): δ 0.80–1.45 (6H, m), 1.58–1.69 (1H, m), 1.70–1.85 (2H, m), 2.05–2.15 (2H, m),

2.20–2.40 (2H, m), 2.65–2.75 (1H, m), 2.92–3.07 (1H, m), 3.24–3.38 (1H, m), 3.45–3.60 (1H, m), 4.17 (1H, m), 4.79 (1H, dd, $J_1 = 10.4$ Hz, $J_2 = 5.9$ Hz), 6.45 (1H, s), 7.29 (1H, d, $J = 7.5$ Hz), 7.45 (1H, t, $J = 7.5$ Hz), 8.26 (1H, d, $J = 7.5$ Hz), 9.14 (2H, br), 9.89 (1H, s). MS (ESI+): m/z 409 (M+H)⁺. HR-MS calcd for C₂₂H₂₉N₆O₂ (M+H)⁺: 409.2352, found 409.2344.

N-(5-Oxo-2,3,5,9b-tetrahydro-1H-pyrrolo[2,1-a]isoindol-9-yl)-N-[5-(pyrrolidin-1-ylmethyl)-1H-pyrazol-3-yl]urea (9g). ¹H NMR (300 MHz, DMSO-*d*₆): δ 0.95–1.10 (1H, m), 1.75–2.10 (4H, m), 2.15–2.40 (2H, m), 2.66–2.78 (1H, m), 3.00–3.20 (2H, m), 3.20–3.65 (4H, m), 4.32 (2H, m), 4.79 (1H, dd, $J_1 = 10.3$ Hz, $J_2 = 5.3$ Hz), 6.43 (1H, s), 7.28 (1H, d, $J = 7.9$ Hz), 7.43 (1H, t, $J = 7.9$ Hz), 8.19 (1H, d, $J = 7.9$ Hz), 9.10 (1H, br), 9.90 (1H, br), 10.63 (1H, br). MS (ESI+): m/z 381 (M+H)⁺. HR-MS calcd for C₂₀H₂₅N₆O₂ (M+H)⁺: 381.2039, found 381.2044.

N-(5-Oxo-2,3,5,9b-tetrahydro-1H-pyrrolo[2,1-a]isoindol-9-yl)-N-[5-(piperidin-1-ylmethyl)-1H-pyrazol-3-yl]urea (9h). ¹H NMR (300 MHz, DMSO-*d*₆): δ 0.80–2.00 (7H, m), 2.15–2.95 (3H, m), 3.20–3.70 (6H, m), 4.25 (2H, m), 4.74 (1H, dd, $J_1 = 10.3$ Hz, $J_2 = 5.3$ Hz), 6.43 (1H, s), 7.27 (1H, d, $J = 7.9$ Hz), 7.42 (1H, t, $J = 7.9$ Hz), 8.17 (1H, d, $J = 7.9$ Hz), 8.90 (1H, br), 9.75 (1H, br). MS (ESI+): m/z 395 (M+H)⁺. HR-MS calcd for C₂₁H₂₇N₆O₂ (M+H)⁺: 395.2195, found 395.2196.

5-[(2S)-1-Benzylpyrrolidin-2-yl]-1H-pyrazol-3-amine (11). To a stirred solution of acetonitrile (0.784 mL, 15.0 mmol) in tetrahydrofuran (25 mL) was added butyllithium (9.6 mL, 1.56 M solution of hexane, 15.0 mmol) at -78 °C. After the solution was stirred for 30 min at the same temperature, *N*-benzyl-L-proline ethyl ester (**10**) (3.18 g, 13.6 mmol) was added. The reaction mixture was stirred at room temperature for 2 h and then poured into water. The solution was acidified by 1 N HCl, neutralized by saturated aqueous NaHCO₃, and extracted with EtOAc. The organic layer was concentrated in vacuo. A solution of the residue (2.73 g) in ethanol (30 mL) was mixed with hydrazine monohydrate (3.0 mL, 61.8 mmol), and the resultant mixture was refluxed for 24 h. The reaction mixture was evaporated in vacuo, and the residue was diluted with CHCl₃ and washed with brine. The organic layer was concentrated in vacuo, and the residue was purified by silica gel column chromatography (5% MeOH in CHCl₃) to give **11** (2.65 g, 81%) as a colorless foam. ¹H NMR (300 MHz, CDCl₃): δ 1.98–2.08 (3H, m), 2.36–2.50 (2H, m), 3.24–3.30 (1H, m), 3.46 (1H, d, $J = 12.9$ Hz), 3.80 (1H, t, $J = 7.3$ Hz), 3.70–4.00 (2H, br), 4.15 (1H, d, $J = 12.9$ Hz), 5.83 (1H, s), 7.48–7.57 (5H, m). MS (ESI+): m/z 243 (M+H)⁺. $[\alpha]_D^{20} -70.2^\circ$ (c 1.0, dimethylformamide).

tert-Butyl 3-Amino-5-[(2S)-1-benzylpyrrolidin-2-yl]-1H-pyrazole-1-carboxylate (12). To a stirred solution of **11** (2.65 g, 10.9 mmol) in dimethylformamide (40 mL) was added NaH (60 wt % in mineral oil, 0.52 g, 13.0 mmol). After the solution was stirred for 30 min at room temperature, di-*tert*-butyl dicarbonate (3.0 mL, 13.1 mmol) was added. The reaction mixture was stirred for 30 min, poured into saturated aqueous NH₄Cl, and extracted with EtOAc. The organic layer was washed with water and brine, dried over MgSO₄, and concentrated in vacuo. The residue was purified by silica gel column chromatography (EtOAc 100%) to give **12** (2.26 g, 61%) as a colorless foam. ¹H NMR (300 MHz, CDCl₃): δ 1.65 (9H, s), 1.74–1.86 (3H, m), 2.12–2.20 (2H, m), 2.86–3.02 (1H, m), 3.13 (1H, d, $J = 13.1$ Hz), 3.47 (1H, t, $J = 7.9$ Hz), 3.93 (1H, d, $J = 12.9$ Hz), 5.24 (2H, brs), 5.57 (1H, s), 7.19–7.31 (5H, m). MS (ESI+): m/z 343 (M+H)⁺. $[\alpha]_D^{20} -21.8^\circ$ (c 1.0, dimethylformamide).

tert-Butyl 5-[(2S)-1-Benzylpyrrolidin-2-yl]-3-[(5-oxo-2,3,5,9b-tetrahydro-1H-pyrrolo[2,1-a]isoindol-9-yl)amino]carbonylamino-1H-pyrazole-1-carboxylate. To a stirred solution of **12** (2.26 g, 6.6 mmol) in tetrahydrofuran (30 mL) was added NaH (60 wt % in mineral oil, 344 mg, 8.6 mmol). After the solution was stirred for 30 min at room temperature, 4-nitrophenyl chloroformate (1.73 g, 8.6 mmol) was added and stirred for an additional 30 min; subsequently, 4-(dimethylamino)pyridine (960 mg, 7.9 mmol) and 9-amino-1,2,3,9b-tetrahydro-5H-pyrrolo[2,1-a]isoindol-5-one²⁵ (1.62 g, 8.6 mmol)

was added. The reaction mixture was stirred for 12 h at 60 °C, poured into 1 N NaOH, and extracted with CHCl₃. The organic layer was washed with brine, dried over MgSO₄, and concentrated in vacuo. The residue was purified by silica gel chromatography (1.5% MeOH in CHCl₃) to give *tert*-butyl 5-[(2S)-1-benzylpyrrolidin-2-yl]-3-[(5-oxo-2,3,5,9b-tetrahydro-1H-pyrrolo[2,1-a]isoindol-9-yl)amino]carbonylamino-1H-pyrazole-1-carboxylate (1.55 g, 42%). ¹H NMR (300 MHz, DMSO-*d*₆): δ 1.01–1.23 (1H, m), 1.64–1.80 (3H, m), 1.65 and 1.69 (each 4.5H, s), 2.00–2.58 (5H, m), 2.59–2.90 (1H, m), 3.17 (1H, d, $J = 13.0$ Hz), 3.43–3.62 (3H, m), 3.78 (1H, d, $J = 13.0$ Hz), 4.64–4.70 (1H, m), 6.43 (1H, brs), 7.20–7.36 (6H, m), 7.43 (1H, t, $J = 8.0$ Hz), 7.55 (1H, d, $J = 8.0$ Hz), 8.35 (1H, d, $J = 8.0$ Hz), 8.70–9.04 (1H, m), 9.96–10.51 (1H, m). MS (ESI+): m/z 557 (M+H)⁺.

N-{5-[(2S)-1-Benzylpyrrolidin-2-yl]-1H-pyrazol-3-yl}-N-(5-oxo-2,3,5,9b-tetrahydro-1H-pyrrolo[2,1-a]isoindol-9-yl)urea (13). *tert*-Butyl 5-[(2S)-1-benzylpyrrolidin-2-yl]-3-[(5-oxo-2,3,5,9b-tetrahydro-1H-pyrrolo[2,1-a]isoindol-9-yl)amino]carbonylamino-1H-pyrazole-1-carboxylate (1.55 g, 2.8 mmol) was diluted with 4 N HCl (MeOH solution, 20 mL), and the resultant solution was stirred for 10 h at room temperature. The mixture was poured into saturated aqueous NaHCO₃, extracted with CHCl₃, washed with brine, dried over MgSO₄, and concentrated in vacuo. The residue was purified by silica gel column chromatography (1.5% MeOH in CHCl₃) to yield **13** (623 mg, 21%). ¹H NMR (300 MHz, DMSO-*d*₆): δ 0.98–1.04 (1H, m), 1.64–1.80 (3H, m), 2.04–2.40 (4H, m), 2.59–2.90 (2H, m), 3.16 (1H, d, $J = 13.2$ Hz), 3.42–3.60 (3H, m), 3.76 (1H, d, $J = 13.2$ Hz), 4.62–4.68 (1H, m), 6.09 (1H, brs), 7.20–7.36 (6H, m), 7.42 (1H, t, $J = 7.9$ Hz), 8.26 (1H, d, $J = 7.9$ Hz), 9.43 (1H, s), 12.40 (1H, s). MS (ESI+): m/z 457 (M+H)⁺. HR-MS calcd for C₂₆H₂₉N₆O₂ (M+H)⁺: 457.2352, found 457.2352. $[\alpha]_D^{20} -46.8^\circ$ (c 1.0, dimethylformamide).

N-[(9bR)-5-Oxo-2,3,5,9b-tetrahydro-1H-pyrrolo[2,1-a]isoindol-9-yl]-N-[5-[(2S)-pyrrolidin-2-yl]-1H-pyrazol-3-yl]urea (14a) and N-[(9bS)-5-Oxo-2,3,5,9b-tetrahydro-1H-pyrrolo[2,1-a]isoindol-9-yl]-N-[5-[(2S)-pyrrolidin-2-yl]-1H-pyrazol-3-yl]urea (14b). To a stirred solution of **13** (620 mg, 1.4 mmol) in MeOH (5.0 mL) were added 4 N HCl (MeOH solution, 0.5 mL) and 10% Pd/C (250 mg). The mixture was stirred at room temperature for 3 days under an atmospheric pressure of hydrogen. The catalyst was removed by filtration, and the filtrate was concentrated in vacuo. The residue was recrystallized from EtOAc–MeOH to give a diastereomeric mixture **14** (264 mg, 51%). A sample of **14** (169 mg) was separated by chiral HPLC (CHIRALPAK AD, 20 ϕ \times 250 mm, ethyl alcohol–ethylamine (1000:1), flow rate 10 mL/min) to give **14a** (retention time 10 min, 45 mg, 99% de) and **14b** (retention time 9 min, 28 mg, 99% de) as white solids. **14a**: mp 223–225 °C. ¹H NMR (300 MHz, DMSO-*d*₆): δ 0.98–1.18 (1H, m), 1.59–1.80 (3H, m), 2.00–2.10 (1H, m), 2.22–2.40 (2H, m), 2.60–2.77 (1H, m), 2.80–2.98 (2H, m), 3.42–3.48 (1H, m), 4.09 (1H, t, $J = 7.2$ Hz), 4.64–4.79 (1H, m), 5.86 (1H, s), 7.26 (1H, d, $J = 6.7$ Hz), 7.42 (1H, dd, $J_1 = 8.0$ Hz, $J_2 = 6.7$ Hz), 8.27 (1H, d, $J = 8.0$ Hz), 9.41 (1H, s), 12.19 (1H, s). MS (ESI+): m/z 367 (M+H)⁺. HR-MS calcd for C₁₉H₂₃N₆O₂ (M+H)⁺: 367.1882, found 367.1895. $[\alpha]_D^{20} 53.2^\circ$ (c 0.5, dimethylformamide). **14b**: mp 229–231 °C. ¹H NMR (300 MHz, DMSO-*d*₆): δ 0.98–1.18 (1H, m), 1.59–1.80 (3H, m), 2.00–2.10 (1H, m), 2.22–2.40 (2H, m), 2.60–2.77 (1H, m), 2.80–2.98 (2H, m), 3.42–3.48 (1H, m), 4.09 (1H, t, $J = 7.2$ Hz), 4.64–4.79 (1H, m), 5.86 (1H, s), 7.26 (1H, d, $J = 6.7$ Hz), 7.42 (1H, dd, $J_1 = 8.0$ Hz, $J_2 = 6.7$ Hz), 8.27 (1H, d, $J = 8.0$ Hz), 9.41 (1H, s), 12.19 (1H, s). MS (ESI+): m/z 367 (M+H)⁺. HR-MS calcd for C₁₉H₂₃N₆O₂ (M+H)⁺: 367.1882, found 367.1892. $[\alpha]_D^{20} -78.4^\circ$ (c 0.5, dimethylformamide).

(+)-N-[(2S)-5-Chloro-2,3-dihydro-1H-inden-2-yl]-4-nitrobenzamide and (–)-N-[(2R)-5-Chloro-2,3-dihydro-1H-inden-2-yl]-4-nitrobenzamide. To a solution of 2-aminoin-dan (14.8 g, 111 mmol) in acetic acid (200 mL) was added Cl₂ gas by bubbling for 5 min at room temperature. After the solution was stirred for 15 min, Cl₂ was removed by the bubbling of N₂ gas. The solution was concentrated in vacuo,

and the residue was washed with hexane–EtOAc (2:1) to yield crude 5-chloro-2,3-dihydro-1*H*-inden-2-ylamine (23 g). To a solution of the crude 5-chloro-2,3-dihydro-1*H*-inden-2-ylamine (23 g) in CHCl₃ was added triethylamine (31 mL, 220 mmol) at room temperature. Subsequently, *p*-nitrobenzoyl chloride (22 g, 120 mmol) was added. After the solution was stirred for 2 h, the reaction mixture was poured into saturated aqueous NaHCO₃ solution. The aqueous layer was extracted with CHCl₃. The combined organic layer was washed with brine, dried over MgSO₄, and concentrated in vacuo. The residue was purified by HPLC (Senshu Pak PEGASIL Silica 60-5, 30φ × 250 mm, hexane–EtOAc (1:1), flow rate 15 mL/min) to give the racemate *N*-(5-chloro-2,3-dihydro-1*H*-inden-2-yl)-4-nitrobenzamide (retention time 13 min, 7.8 g, 22%). *N*-(5-chloro-2,3-dihydro-1*H*-inden-2-yl)-4-nitrobenzamide (7.8 g) was separated by chiral HPLC (CHIRALCEL OD, 20φ × 250 mm, hexane–isopropyl alcohol (2:3), flow rate 10 mL/min) to yield (+)-*N*-[(2*S*)-5-chloro-2,3-dihydro-1*H*-inden-2-yl]-4-nitrobenzamide (retention time 17 min, 3.63 g, 99% ee) and (–)-*N*-[(2*R*)-5-chloro-2,3-dihydro-1*H*-inden-2-yl]-4-nitrobenzamide (retention time 14 min, 3.76 g, 99% ee) as white solids.

(+)-*N*-[(2*S*)-5-Chloro-2,3-dihydro-1*H*-inden-2-yl]-4-nitrobenzamide: mp 168–170 °C. ¹H NMR (300 MHz, DMSO-*d*₆): δ 2.88 (1H, t, *J* = 5.2 Hz), 2.97 (1H, t, *J* = 5.2 Hz), 3.39 (1H, dd, *J*₁ = 6.0 Hz, *J*₂ = 5.2 Hz), 3.47 (1H, dd, *J*₁ = 6.0 Hz, *J*₂ = 5.2 Hz), 4.88–5.05 (1H, m), 6.29–6.42 (1H, m), 7.17–7.31 (3H, m), 7.89 (1H, d, *J* = 8.6 Hz), 8.27 (1H, d, *J* = 8.6 Hz). HR-MS calcd for C₁₆H₁₄N₂O₃³⁵Cl (M+H)⁺: 317.0693, found 317.0696. [α]_D²⁰ 52.4° (c 1.0, CHCl₃).

(–)-*N*-[(2*R*)-5-Chloro-2,3-dihydro-1*H*-inden-2-yl]-4-nitrobenzamide: mp 168–170 °C. ¹H NMR (300 MHz, DMSO-*d*₆): δ 2.88 (1H, t, *J* = 5.2 Hz), 2.97 (1H, t, *J* = 5.2 Hz), 3.39 (1H, dd, *J*₁ = 6.0 Hz, *J*₂ = 5.2 Hz), 3.47 (1H, dd, *J*₁ = 6.0 Hz, *J*₂ = 5.2 Hz), 4.88–5.05 (1H, m), 6.29–6.42 (1H, m), 7.17–7.31 (3H, m), 7.89 (1H, d, *J* = 8.6 Hz), 8.27 (1H, d, *J* = 8.6 Hz). HR-MS calcd for C₁₆H₁₄N₂O₃³⁵Cl (M+H)⁺: 317.0693, found 317.0698. [α]_D²⁰ –50.2° (c 1.0, CHCl₃).

***N*-[(9*bR*)-5-Oxo-2,3,5,9*b*-tetrahydro-1*H*-pyrrolo[2,1-*a*]isoindol-9-yl]-*N*-[5-(([(2*S*)-5-chloro-2,3-dihydro-1*H*-inden-2-yl]amino)methyl)-1*H*-pyrazol-3-yl]urea (15*a*) and *N*-[(9*bS*)-5-Oxo-2,3,5,9*b*-tetrahydro-1*H*-pyrrolo[2,1-*a*]isoindol-9-yl]-*N*-[5-(([(2*S*)-5-chloro-2,3-dihydro-1*H*-inden-2-yl]amino)methyl)-1*H*-pyrazol-3-yl]urea (15*b*).** To a solution of (+)-*N*-[(2*S*)-5-chloro-2,3-dihydro-1*H*-inden-2-yl]-4-nitrobenzamide (1.52 g, 4.79 mmol) in 12 N HCl (160 mL) was added acetic acid (30 mL). The resultant mixture was refluxed for 10 h. After cooling to room temperature, the reaction mixture was diluted with CHCl₃ and extracted with water. The combined aqueous layer was made alkaline with 12 N NaOH to pH 11 and extracted with CHCl₃. The combined organic layer was washed by brine, dried over MgSO₄, and concentrated in vacuo to produce crude (2*S*)-5-chloro-2,3-dihydro-1*H*-inden-2-amine (0.29 g, 36%). A solution of **8** (0.50 g, 1.5 mmol) in CHCl₃–MeOH (1:1, 10 mL) was mixed with crude (2*S*)-5-chloro-2,3-dihydro-1*H*-inden-2-amine (0.29 g, 1.7 mmol). The resultant mixture was stirred for 10 h at 50 °C. After the solution was cooled to room temperature, NaBH₄ (87 mg, 2.3 mmol) was added, and the mixture was stirred for 1 h. The mixture was poured into saturated aqueous NH₄Cl and extracted with CHCl₃. The combined organic layer was washed with brine, dried over MgSO₄, and concentrated in vacuo. The residue was purified by preparative silica gel chromatography (Merck Art.5744, 10% MeOH in CHCl₃) to give a diastereomeric mixture of *N*-(5-oxo-2,3,5,9*b*-tetrahydro-1*H*-pyrrolo[2,1-*a*]isoindol-9-yl)-*N*-[5-(([(2*S*)-5-chloro-2,3-dihydro-1*H*-inden-2-yl]amino)methyl)-1*H*-pyrazol-3-yl]urea (0.25 g, 34%) as a white solid. *N*-(5-Oxo-2,3,5,9*b*-tetrahydro-1*H*-pyrrolo[2,1-*a*]isoindol-9-yl)-*N*-[5-(([(2*S*)-5-chloro-2,3-dihydro-1*H*-inden-2-yl]amino)methyl)-1*H*-pyrazol-3-yl]urea (0.25 g) was separated by chiral HPLC (CHIRALPAK AD, 20φ × 250 mm, ethyl alcohol 100%, flow rate 15 mL/min) to yield **15a** (retention time 15 min, 109 mg, 100% de) and **15b** (retention time 22 min, 113 mg, 100% de) as white solids. **15a**: mp 214–215 °C. ¹H NMR (300 MHz, DMSO-*d*₆): δ 0.98–1.14 (1H, m), 2.23–2.40 (1H, m), 2.59–

2.80 (3H, m), 2.98–3.18 (2H, m), 3.22–3.60 (3H, m), 3.71 (2H, s), 4.63–4.78 (1H, m), 6.08 (1H, s), 7.08–7.22 (3H, m), 7.24 (1H, d, *J* = 6.5 Hz), 7.44 (1H, dd, *J*₁ = 7.9 Hz, *J*₂ = 6.5 Hz), 8.27 (1H, d, *J* = 7.9 Hz), 9.43 (1H, s), 12.22 (1H, s). MS (ESI⁺): *m/z* 477 (M+H)⁺. HR-MS calcd for C₂₅H₂₆N₆O₂Cl (M+H)⁺: 477.1806, found 477.1800. [α]_D²⁰ 72.2° (c 1.0, dimethylformamide). Anal. (C₂₅H₂₅N₆O₂Cl·1H₂O) C, H, N. **15b**: mp 215–217 °C. ¹H NMR (300 MHz, DMSO-*d*₆): δ 0.98–1.14 (1H, m), 2.23–2.40 (1H, m), 2.59–2.80 (3H, m), 2.98–3.18 (2H, m), 3.22–3.60 (3H, m), 3.71 (2H, s), 4.63–4.78 (1H, m), 6.08 (1H, s), 7.08–7.22 (3H, m), 7.24 (1H, d, *J* = 6.5 Hz), 7.44 (1H, dd, *J*₁ = 7.9 Hz, *J*₂ = 6.5 Hz), 8.27 (1H, d, *J* = 7.9 Hz), 9.43 (1H, s), 12.22 (1H, s). MS (ESI⁺): *m/z* 477 (M+H)⁺. HR-MS calcd for C₂₅H₂₆N₆O₂Cl (M+H)⁺: 477.1806, found 477.1805. [α]_D²⁰ –62.4° (c 1.0, dimethylformamide). Anal. (C₂₅H₂₅N₆O₂Cl·1H₂O) C, H, N.

Molecular Modeling. Computer calculations were performed on a Silicon Graphics Octane. Molecular mechanics calculations were carried out using the CHARMM force field. The distance-dependent dielectric constant ε = 1 was used. The Docking studies were performed using modeling software QUANTA (QUANTA Modeling Environment, December 1998, San Diego: Molecular Simulations Inc., 1998). Initial docking models between the Cdk2/4 and inhibitors (**1**, **2a**, **9d**, and **15b**) were achieved by manual docking based on the X-ray structures of Cdk2–**1** complex and Cdk4 mimic Cdk2–**14b** complex.⁹ Subsequently, 200–400 conformations were generated using random sampling, following minimization for each initial model. These conformations were clustered using the RMSD of atomic coordinates (ca. 15–30 clusters). The most preferable conformations were selected by considering energy, status of hydrogen-bonds, and van der Waals contacts between hydrophobic surfaces. Candidates of the substituent on the pyrazole ring of **2a** were generated by the *de novo* design programs, LUDI¹⁹ and LeapFrog.²⁰ The docking model of Cdk4–**2a** was used as a seed structure for *de novo* design, and the 5-position of the pyrazole ring in **2a** was selected as a substitution point.

Cdk Assays (Cyclin D₂–Cdk4, Cyclin D₁–Cdk6, Cyclin A–Cdk2, and Cyclin B–Cdk1). In vitro Cdk assays were performed as previously described²⁶ with some modifications. A recombinant human cyclin D₂–Cdk4, cyclin D₁–Cdk6, or cyclin A–Cdk2 complexes were expressed in Sf9 cells with a baculovirus expression system and purified using HPLC. Recombinant human cyclin B–Cdk1 was purchased from Promega Corporation (USA). The purified Cdk4s were incubated with 50 μM ATP (0.5–1.5 μCi of [³³P]-ATP (3000 Ci/mmol)), 100 μM or 400 μM G1 peptide (for Cdk4/6) or 10 mg/mL of S1 peptide (for Cdk1/2), R buffer (20 mM Tris-HCl pH 7.4, 10 mM MgCl₂, 4.5 mM 2-mercaptoethanol, 1 mM EGTA), and diluted compounds at 30 °C for 20 min (for Cdk6) or 45 min (for Cdk1/2/4). The reactions were terminated by the addition of 350 mM H₃PO₄. Peptides were trapped and washed using P81 paper filter 96-well plates (Millipore) and 75 mM H₃PO₄. ³³P incorporation was measured with a Top Count (Packard).

Other Ser/Thr Kinase Assays. PKA, PKC, PKBα, CaMK II, p38α, ERK1, and MEK1 were assayed in MDS pharma Services.²⁷

Tyr Kinase Assays. Src, Lck, Flt-1, ZAP, EGFR, FGFR1, and PFGFRβ were assayed in the Merck research laboratory.²⁸

Acknowledgment. It is our pleasure to acknowledge the contributions of Dr. Toshiyasu Shimomura and of Mr. Takumitsu Machida (for cell assay), Miss Hiroko Oki (for Cdk4 inhibitory assay), Mr. Hirokazu Ohsawa (for mass spectral analysis), Mrs. Chihiro Sato (for elemental analysis), and Dr. Kenji Kamata (for X-ray analysis). We thank Mr. Toshiharu Iwama, Dr. Hiroshi Funabashi, Dr. Hiroshi Hirai, and Dr. Takehiro Fukami for their useful suggestions. We are also grateful to Miss Jocelyn Winward for her critical reading of this manuscript.

References

- (1) Pines, J. Cyclins and cyclin-dependent kinases: take your partners. *Trends Biochem. Sci.* **1993**, *18*, 195–197.
- (2) Sherr, C. J. D-type cyclins. *Trends Biochem. Sci.* **1995**, *20*, 187–190.
- (3) (a) Taya, Y. Cell cycle-dependent phosphorylation of the tumor suppressor RB protein. *Mol. Cells* **1995**, *5*, 191–195. (b) Weinberg, R. A. The retinoblastoma protein and a cell cycle control. *Cell* **1995**, *81*, 323–330. (c) Kato, J.; Matsushime, H.; Hiebert, S. W.; Ewen, M. E.; Sherr, C. J. Direct binding of cyclin D to the retinoblastoma gene product (pRB) and pRB phosphorylation by the cyclin D-dependent kinase CDK4. *Genes Dev.* **1993**, *7*, 331–342. (d) Baldin, V.; Lukas, J.; Marcote, M. J.; Pagano, M.; Draetta, G. Cyclin D1 is nuclear protein required for cell cycle progression in G1. *Genes Dev.* **1993**, *7*, 812–821.
- (4) Kamb, A. Cell-cycle regulators and cancer. *Trends Genet.* **1995**, *11*, 136–140.
- (5) Fry, D. W.; Garret, M. D. Inhibitors of cyclin-dependent kinases as therapeutic agents for the treatment of cancer. *Curr. Opin. Oncol. Endocr. Metab. Invest. Drugs* **2000**, *2*, 40–59.
- (6) Honma, T.; Hayashi, K.; Aoyama, T.; Hashimoto, N.; Machida, T.; Fukasawa, K.; Iwama, T.; Ikeura, C.; Ikuta, M.; Suzuki-Takahashi, I.; Iwasawa, Y.; Hayama, T.; Nishimura, S.; Morishima, H. Structure-based generation of a new class of potent Cdk4 inhibitors: new *de novo* design strategy and library design. *J. Med. Chem.* **2001**, *44*, 4615–4627.
- (7) Russo, A. A.; Jeffrey, P. D.; Pavletich, N. P. Structural basis of cyclin-dependent kinase activation by phosphorylation. *Nat. Struct. Biol.* **1996**, *3*, 696–700.
- (8) Iwama, T.; Honma, T.; Ikeura, C. System for evaluation of availability of essential structures generated by *de novo* design programs (SEEDS). Unpublished results.
- (9) Ikuta, M.; Kamata, K.; Fukasawa, K.; Honma, T.; Machida, T.; Hirai, H.; Suzuki-Takahashi, I.; Hayama, T.; Nishimura, S. Crystallographic approach to identification of cyclin dependent kinase 4 (CDK4) specific inhibitors by using CDK4 mimic CDK2 protein. *J. Biol. Chem.* **2001**, *276*, 27548–27554.
- (10) (a) Nurse, P. Universal control mechanism regulating onset of M-phase. *Nature* **1990**, *344*, 503–508. (b) Johnson, D. G.; Walker, C. L. Cyclins and cell cycle check-points. *Annu. Rev. Pharmacol. Toxicol.* **1999**, *39*, 295–312.
- (11) (a) Pardee, A. B. A restriction point for control of normal animal cell proliferation. *Proc. Natl. Acad. Sci. U.S.A.* **1974**, *71*, 1286–1290. (b) Pardee, A. B.; Durbrow, R.; Hamlin, J. L.; Kletzien, R. F. Animal cell cycle. *Annu. Rev. Biochem.* **1978**, *47*, 715–750.
- (12) (a) Chen, J. M.; Nelson, F. C.; Levin, J. I.; Mobilio, D.; Moy, F. J.; Nilakantan, R.; Zask, A.; Powers, R. Structure-based design of a novel, potent, and selective inhibitor for MMP-13 utilizing NMR spectroscopy and computer-aided molecular design. *J. Am. Chem. Soc.* **2000**, *122*, 9648–9654. (b) Iversen, L. F.; Andersen, H. S.; Branner, S.; Mortensen, S. B.; Peters, G. H.; Norris, K.; Olsen, O. H.; Jeppesen, C. B.; Lundt, B. F.; Ripka, W.; Moller, K. B.; Moller, N. P. H. Structure-based design of a low molecular weight, nonphosphorus, nonpeptide, and highly selective inhibitor of protein-tyrosine phosphatase 1B. *J. Biol. Chem.* **2000**, *275*, 10300–10307. (c) Bayly, C. I.; Black, W. C.; Leger, S.; Ouimet, N.; Ouellet, M.; Percival, M. D. Structure-based design of COX-2 selectivity into flurbiprofen. *Bioorg. Med. Chem. Lett.* **1999**, *9*, 307–312. (d) Kurumbail, R. G.; Stevens, A. M.; Gierse, J. K.; McDonald, J. J.; Stegeman, R. A.; Pak, J. Y.; Gildehaus D.; Miyashiro, J. M.; Penning, T. D.; Seibert, K.; Isakson, P. C.; Stallings, W. C.; Structural basis for selective inhibition of cyclooxygenase-2 by antiinflammatory agents. *Nature* **1996**, *384*, 644–648.
- (13) (a) Hanks, S. K.; Quinn, A. M.; Hunter, T. The protein kinase family: conserved features and deduced phylogeny of the catalytic domains. *Science* **1988**, *241*, 42–52. (b) Hanks, S. K.; Quinn, A. M. Protein kinase catalytic domain sequence database: identification of conserved features of primary structure and classification of family members. *Methods Enzymol.* **1991**, *200*, 38–62. (c) Hanks, S. K.; Hunter, T. Protein kinases. 6. The eukaryotic protein kinase superfamily: kinase (catalytic) domain structure and classification. *FASEB J.* **1995**, *9*, 576–96. (d) Also see a review: Toledo, L. M.; Lydon, N. B.; Elbaum, D.; The structure-based design of ATP-site directed protein kinase inhibitors. *Curr. Med. Chem.* **1999**, *6*, 775–805.
- (14) http://www.nih.gov/mirror/Kinases/pkr/pk_catalytic/pk_hanks_seq_align_long.html.
- (15) Atherton-fessler S.; Parker L. L.; Geahlen R. L.; Piwnica-worms H. Mechanisms of p38cdc2 Regulation. *Mol. Cell. Biol.* **1993**, *13*, 1675–1685.
- (16) (a) Russo, A. A.; Tong, L.; Lee, J.-O.; Jeffrey, P. D.; Pavletich, N. P. Structural basis for inhibition of the cyclin-dependent kinase Cdk6 by the tumor suppressor p16INK4a. *Nature* **1998**, *395*, 237–243. (b) Jeffrey, P. D.; Tong, L.; Pavletich, N. P. Structural basis of inhibition of CDK-cyclin complexes by INK4 inhibitors. *Genes Dev.* **2000**, *14*, 3115–3125. (c) Brotherton, D. H.; Dhanaraj, V.; Wick, S.; Leonardo, B.; Domaille, P. J.; Volyanik, E.; Xu, X.; Parisini, E.; Smith, B. O.; Archher, S. J.; Serrano, M.; Brenner, S. L.; Blundell, T. L.; Laue, E. D. Crystal structure of the complex of the cyclin D-dependent kinase Cdk6 bound to the cell-cycle inhibitor p19INK4d. *Nature* **1998**, *395*, 244–250.
- (17) (a) Lukas, J.; Parry, D.; Aagaard, L.; Mann, D. J.; Bartkova, J.; Stauss, M.; Peters, G.; Bartek, J. Retinoblastoma-protein-dependent cell-cycle inhibition by the tumor suppressor p16. *Nature* **1995**, *375*, 503–506. (b) Koh, J.; Enders, G. H.; Dynlacht, B. D.; Harlow, E. Tumor-derived p16 encoding proteins defective in cell-cycle inhibition. *Nature* **1995**, *375*, 506–508.
- (18) Reviewed in Murcko M. A. An introduction to *de novo* ligand design. In *Practical Application of Computer-aided Drug Design*; Charifson, P. S., Ed.; Marcel Dekker: New York, 1997; pp 304–354.
- (19) (a) Boehm, H. J. The computer program LUDI: a new method for the *de novo* design of enzyme inhibitors. *J. Comput.-Aided Mol. Des.* **1992**, *6*, 61–78. (b) Boehm H. J. LUDI: rule-based automatic design of new substituents for enzyme inhibitor leads. *J. Comput.-Aided Mol. Des.* **1992**, *6*, 593–606.
- (20) LeapFrog manual, SYBYL version 6.1, Tripos Associates, St. Louis, MO.
- (21) Elnagdi, M. H.; Abdel-Galil, F. M.; Riad, B. Y.; Elgemeie, G. E. H. Recent developments in the chemistry of 3(5)-aminopyrazoles. *Heterocycles* **1983**, *20*, 2437–2470.
- (22) The absolute configuration of **14a** was confirmed by synthesis of **14a** from (–)-*N*-benzyl-L-proline ethyl ester and (+)-(9*bR*)-9-amino-1,2,3,9b-tetrahydro-5*H*-pyrrolo[2,1-*a*]isoindol-5-one.⁶ The absolute configuration of **15a** was confirmed by synthesis of **15a** from (+)-(9*bR*)-9-amino-1,2,3,9b-tetrahydro-5*H*-pyrrolo[2,1-*a*]isoindol-5-one⁶ and (+)-(2*S*)-5-chloro-2,3-dihydro-1*H*-inden-2-amine. The absolute configuration of (–)-(2*R*)-5-chloro-2,3-dihydro-1*H*-inden-2-amine was determined by X-ray analysis.
- (23) Hirai, H.; Fukasawa, K.; Machida, T.; Shimomura, T.; Oki, H.; Honma, T.; Hayashi, K.; Yoshizumi, T.; Hayama, T.; Suzuki-Takahashi, I. Effects of diarylurea class of Cdk4 selective inhibitor on the progression of mammalian cell cycle. Unpublished results.
- (24) Ege, G.; Arnord, P. Aminopyrazole; II. C-Unsubstituierte 1-alkyl-3-aminopyrazole aus 2-chloroacrylnitril bzw. 2,3-dichloropropanitril und alkylhydrazinen. *Synthesis* **1976**, *1*, 52–53.
- (25) Hammond, K. M.; Fisher, N.; Morgan, E. N.; Tanner, E. M.; Franklin, C. S. 3:5-Dioxo-1:2-diphenylpyrazolidines. The 4-hydroxy- and certain 4-alkoxy- and 4-alkylamino-analogues. *J. Chem. Soc.* **1957**, 1062–1067.
- (26) (a) Kitagawa, M.; Okabe, T.; Ogino, H.; Matsumoto, H.; Suzuki-Takahashi, I.; Kokubo, T.; Higashi, H.; Saitoh, S.; Taya, Y.; Yasuda, H.; Ohba, Y.; Nishimura, S.; Tanaka, N.; Okuyama, A. Butyrolactone I, a selective inhibitor of cdk2 and cdc2 kinase. *Oncogene* **1993**, *8*, 2425–2432. (b) Kitagawa, M.; Higashi, H.; Jung, H.-K.; Suzuki-Takahashi, I.; Ikeda, M.; Tamai, K.; Kato, J.; Segawa, K.; Yoshida, E.; Nishimura, S.; Taya, Y. The consensus motif for phosphorylation by cyclin D1-Cdk4 is different from that for phosphorylation by cyclin A/E-Cdk2. *EMBO J.* **1996**, *15*, 7060–7069.
- (27) MDS Pharma Services Discovery, WA.
- (28) Park, Y.-W.; Cummings, R. T.; Wu, L.; Zheng, S.; Cameron, P. M.; Woods, A.; Zaller, D. M.; Marcy, A. I.; Hermes, J. D. Homogeneous proximity tyrosine kinase assays: scintillation proximity assay versus homogeneous time-resolved fluorescence. *Anal. Biochem.* **1999**, *269*, 94–104.

JM010326Y